CaMKII enhances voltage-gated sodium channel Nav1.6 activity and neuronal excitability

Received for publication, April 24, 2020, and in revised form, June 30, 2020 Published, Papers in Press, July 1, 2020, DOI 10.1074/jbc.RA120.014062

Agnes S. Zybura[1], **Anthony J. Baucum II**[1,2], **Anthony M. Rush**[3], **Theodore R. Cummins**[1,2], **and Andy Hudmon**[1,4,*]

From the [1]*Program in Medical Neuroscience, Paul and Carole Stark Neurosciences Research Institute, Indiana University School of Medicine, Indianapolis, Indiana, USA, the* [2]*Biology Department, Indiana University–Purdue University Indianapolis, School of Science, Indianapolis, Indiana, USA,* [3]*Metrion Biosciences Limited, Cambridge, United Kingdom, and the* [4]*Department of Medicinal Chemistry and Molecular Pharmacology, Purdue University, West Lafayette, Indiana, USA*

Edited by Mike Shipston

Nav1.6 is the primary voltage-gated sodium channel isoform expressed in mature axon initial segments and nodes, making it critical for initiation and propagation of neuronal impulses. Thus, Nav1.6 modulation and dysfunction may have profound effects on input-output properties of neurons in normal and pathological conditions. Phosphorylation is a powerful and reversible mechanism regulating ion channel function. Because Nav1.6 and the multifunctional Ca^{2+}/CaM-dependent protein kinase II (CaMKII) are independently linked to excitability disorders, we sought to investigate modulation of Nav1.6 function by CaMKII signaling. We show that inhibition of CaMKII, a Ser/Thr protein kinase associated with excitability, synaptic plasticity, and excitability disorders, with the CaMKII-specific peptide inhibitor CN21 reduces transient and persistent currents in Nav1.6-expressing Purkinje neurons by 87%. Using whole-cell voltage clamp of Nav1.6, we show that CaMKII inhibition in ND7/23 and HEK293 cells significantly reduces transient and persistent currents by 72% and produces a 5.8-mV depolarizing shift in the voltage dependence of activation. Immobilized peptide arrays and nanoflow LC-electrospray ionization/MS of Nav1.6 reveal potential sites of CaMKII phosphorylation, specifically Ser-561 and Ser-641/Thr-642 within the first intracellular loop of the channel. Using site-directed mutagenesis to test multiple potential sites of phosphorylation, we show that Ala substitutions of Ser-561 and Ser-641/Thr-642 recapitulate the depolarizing shift in activation and reduction in current density. Computational simulations to model effects of CaMKII inhibition on Nav1.6 function demonstrate dramatic reductions in spontaneous and evoked action potentials in a Purkinje cell model, suggesting that CaMKII modulation of Nav1.6 may be a powerful mechanism to regulate neuronal excitability.

The voltage-gated sodium channel (Nav) family is a class of ion channels that is critical for generating and propagating action potentials (AP). Navs are large heteromultimeric protein complexes that are formed by α subunits, which are the functional pore-forming subunits of the channel, and one or more auxiliary β subunits. Sodium channel α subunits are encoded by 10 genes that control expression in various excitable cells (1). In the brain, the isoform Nav1.6 is critical for regulating and maintaining neuronal excitability (2). Nav1.6 is unique both in its expression pattern and biophysical properties. In adult neurons, Nav1.6 is predominantly expressed at the axon initial segment (AIS), the proximal unmyelinated region of the neuron where APs are initiated (3), and at nodes of Ranvier, where APs are propagated down the axon (3, 4). This provides Nav1.6 with significant control of AP initiation as well as propagation of neuronal impulses (3, 5). Furthermore, Nav1.6 displays unique biophysical properties that enable the channel to exert powerful tuning capabilities of these impulses. For example, Nav1.6 can generate large persistent currents (6–8), which is an atypical form of sodium current activity that may profoundly impact the physiology of excitable cells (9, 10).

Changes in Nav1.6 expression and function are associated with excitability disorders including neuropathic pain (11–13), epilepsies (2, 6, 14–16), autism-spectrum disorders (17, 18), ischemia (19), and stress-induced changes in signal transduction (20, 21). Notably, many of these changes are significantly influenced by intracellular mediators, including protein-protein interactions and post-translational modifications. Phosphorylation is a powerful mechanism that can rapidly modulate Nav function and expression. The most widely studied phosphorylation-mediated modulation of neuronal Navs has focused on the roles of protein kinases A and C (22–26) and p38 mitogen-activated protein kinase (20, 27) in excitatory dysregulation. Dysfunction in αCaMKII activity is also significantly linked to excitatory disorders and is highly co-localized with Navs in neurons (28–32). CaMKII, therefore, may be contributing to pro-excitatory changes within the brain by modulating the activity of neuronal Navs. However, CaMKII phosphorylation and modulation of Nav1.6, the major isoform critical for AP initiation and propagation, has not been investigated.

CaMKII is a multifunctional serine/threonine protein kinase highly concentrated in the brain and is critical for neuronal excitability (33). There are four genes that encode mammalian subunits, with the α subunit predominating in excitatory neurons of the forebrain and Purkinje neurons of the cerebellum (34, 35). During excitatory events, CaMKII is transiently activated upon calcium influx and may retain persistent activity (36–38), providing CaMKII with a unique capability to decode these events and form molecular memory of its activation (39–42). Fluctuations in CaMKII activity are often associated with neuronal diseases, including epilepsy and autism-spectrum disorders (32), ischemia (43, 44), and pain (45–47). Previous

This article contains supporting information.

* For correspondence: Andy Hudmon, ahudmon@purdue.edu.

studies suggest that coupling between CaMKII and Navs contributes to regulation of neuronal excitability (28, 30). To this end, CaMKII inhibition has been shown to reduce excitability of small and medium trigeminal ganglion neurons in addition to decreasing sodium current amplitude (48). Moreover, CaMKII inhibition also reduces sodium current amplitude in cerebellar granule cells (49), in which Nav1.6 is the predominant isoform (10). These studies suggest that CaMKII signaling may play a major role in neuronal excitability, possibly through modulation of Nav1.6 sodium currents.

In this study, we directly investigate the potential for CaMKII to phosphorylate and modulate Nav1.6. Multiple biochemical approaches, including MS and immobilized peptide arrays, were used to identify CaMKII phosphorylation sites on Nav1.6, and whole-cell voltage-clamp electrophysiology was used to examine the functional effects of this phosphorylation on channel biophysical properties. Using computational simulations, we further sought to examine how functional changes in Nav1.6 induced by CaMKII modulation may impact spontaneous and evoked AP initiation in neurons.

Results

Effects of CaMKII inhibition on sodium currents in Purkinje neurons

Electrophysiological recordings of bulk sodium currents from trigeminal neurons and cerebellar granule cells show significantly decreased transient sodium currents following CaMKII inhibition with KN93 or KN62 (48, 49). To further explore the potential for CaMKII to regulate sodium currents in neurons, we recorded from Purkinje cells incubated with the CaMKII inhibitor CN21 conjugated to the tat cell–penetrating motif (tatCN21) or its inactive analog tatCN21Ala (50). Sodium currents from Purkinje cells treated with no peptide (*left*), tatCN21 (*middle*), or tatCN21Ala (*right*) were elicited with a series of depolarizing steps ranging from −100 to +15 mV for 50 ms from a holding potential of −100 mV (Fig. 1*A*). Application of tatCN21 to inhibit CaMKII significantly reduced transient sodium current density by 87% (Fig. 1*C*) in Purkinje neurons compared with no peptide or tatCN21Ala-treated cells. We also examined persistent current generation in Purkinje neurons in the context of CaMKII inhibition by using the same depolarizing step protocol as described above. Persistent current is a noninactivating, or very slowly inactivating, sodium current and was measured at the end of the current trace (Fig. 1*B*). These currents are known to amplify subthreshold inputs and mediate repetitive action potential firing (9, 51, 52). In addition to decreasing transient sodium currents in Purkinje neurons, CaMKII inhibition with tatCN21 also reduces persistent current density (Fig. 1*D*). Current densities were calculated by normalizing the current amplitude at −25 mV by the cell capacitance. We used −25 mV for transient and persistent sodium current measurements to minimize clamp error artifacts during analysis. We did not determine the impact of CaMKII inhibition on Purkinje neuron sodium current voltage dependence because of issues with space-clamp errors. Because Nav1.6 is the predominant sodium current observed in Purkinje neurons (53), these data suggest that Nav1.6 may be a substrate for CaMKII and modulated by CaMKII signaling.

Biophysical characterization of CaMKII effects on Nav1.6 activity

While Nav1.6 is the predominant sodium current in Purkinje neurons (53), it is conceivable that the expression of another tetrodotoxin (TTX)-sensitive voltage-gated sodium channel isoform (*e.g.* Nav1.1) in Purkinje neurons could contaminate our recordings. The TTX metabolite 4,9-anhydro-TTX has been reported to selectively target Nav1.6 sodium currents (54). However, recent evidence shows that 4,9-anhydro-TTX also blocks Nav1.1 currents at similar concentrations required to block Nav1.6 activity (55). Therefore, we turned to a heterologous expression system, where the role of CaMKII in modulating Nav1.6 sodium currents could be explored without significant contamination from other endogenous voltage-gated sodium channel isoforms. Whole-cell voltage-clamp recordings were obtained in neuronal ND7/23 cells transiently co-transfected with GFP (positive selection) and a tetrodotoxin-resistant (TTX-R) form (Y371S point mutation) of the human Nav1.6 channel that makes Nav1.6 resistant to TTX, yet does not appear to alter its biophysical properties (56). In this system, TTX can be used to block endogenous currents, allowing TTX-R Nav1.6 current to be effectively studied in isolation. Space- and voltage-clamp errors are also more effectively controlled in ND7/23 cells. The CaMKII peptide inhibitor CN21 or its inactive analog, CN21Ala, was included in the patch pipette. Whereas we observed 15.9 ± 1.9% autonomously active CaMKII in our cultured ND7/23 cells (see "Experimental procedures"), we also included Ca^{2+} and calmodulin in the patch pipette to promote further activation of endogenous CaMKII as described previously (57). A representative family of current traces for WT human Nav1.6 treated with no peptide (*left*), CN21 (*middle*), or CN21Ala (*right*) that were elicited with a series of depolarizing steps ranging from −80 to +60 mV for 50 ms from a holding potential of −80 mV are shown in Fig. 2*A*. Endogenous CaMKII inhibition with CN21 resulted in a 72% decrease in Nav1.6 transient current density compared with no peptide or CN21Ala control treatments (Fig. 2*B*). Representative families of persistent current traces are shown in Fig. 3*A* with the percentage of persistent current-voltage curves shown on the *left* in Fig. 3*B* and the peak current density values plotted on the *right*. We observed a significant down-regulation of persistent current density with CN21 treatment (72% reduction), a reduction proportional to the decrease observed in the peak transient current. As a complementary approach, we also recorded sodium currents from HEK293 cells stably expressing recombinant TTX-R human Nav1.6 and, as with ND7/23 cells, observed significant reductions in Nav1.6 transient and persistent current densities with CaMKII inhibition (Fig. S1). We used 0 mV for peak sodium current measurements in both ND7/23 and HEK293 cells because the sodium current voltage dependence is shifted to more positive values in these cell types. Thus, consistent with our data in Purkinje neurons, we

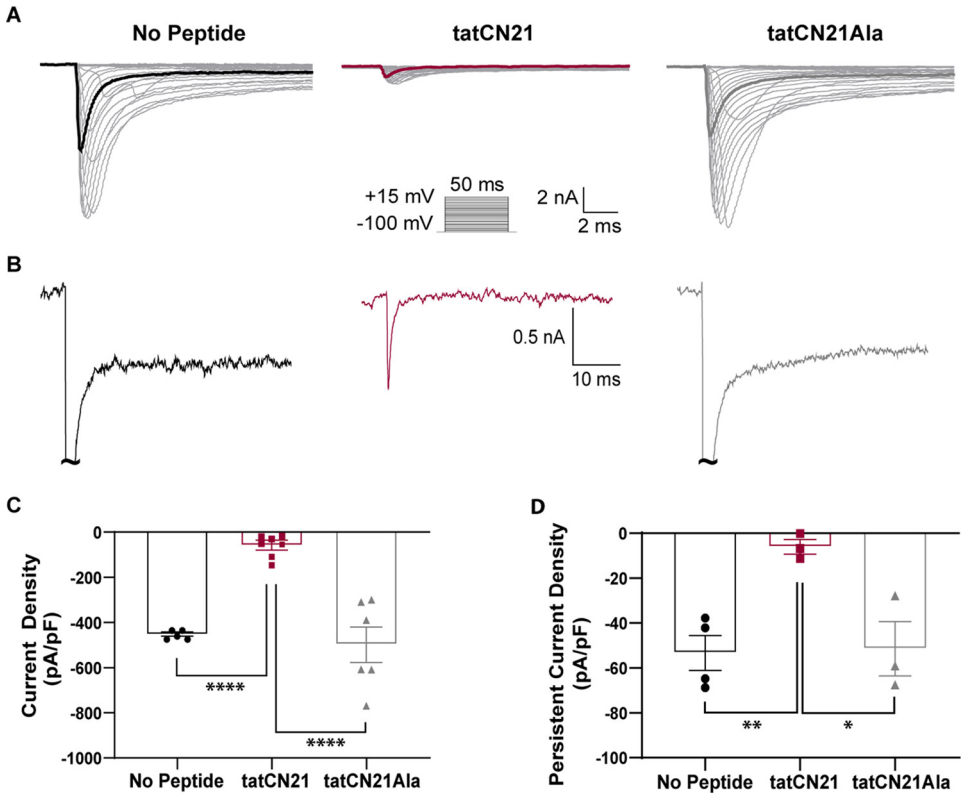

Figure 1. CaMKII inhibition reduces sodium currents in acutely dissociated Purkinje neurons. Shown are a representative family of transient (*A*) and persistent (*B*) sodium current traces recorded from acutely dissociated Purkinje neurons with no peptide (*left*, *black*), tatCN21 (*middle*, *red*), and tatCN21Ala (*right*, *gray*). *Boldface traces* represent sodium current at −25 mV. *C*, transient current density values (−25 mV). $F(2, 326) = 44.5$, $p < 0.0001$ by two-way ANOVA performed across voltages ranging from −100 to +15 mV. *D*, persistent current density values (−25 mV). $F(2, 72) = 13.45$, $p < 0.0001$ by two-way ANOVA performed across voltages ranging from −65 to −15 mV. *, $p < 0.05$; **, $p < 0.01$; ****, $p < 0.0001$. $n = 3–7$. Two-way ANOVA ± S.E. (*error bars*), Tukey's post hoc test. *pF*, picofarads.

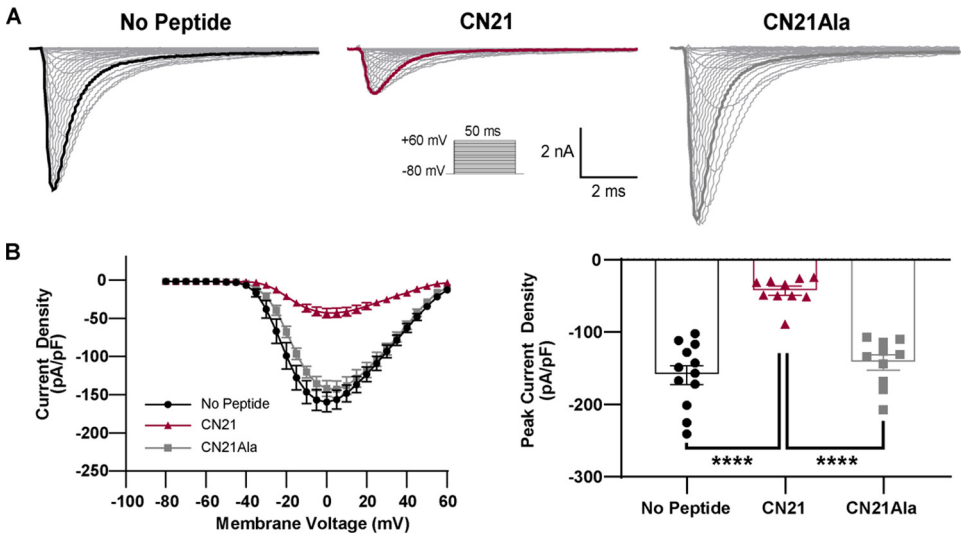

Figure 2. CaMKII inhibition reduces Nav1.6 transient current density. *A*, representative family of transient current traces generated by TTX-R hNav1.6 transiently expressed in ND7/23 cells recorded with no peptide (*right*), CN21 (*middle*), and CN21Ala (*right*) in the patch pipette. Currents were elicited with 50-ms step depolarizations ranging from −80 to +60 mV (*inset*). Peak current traces (0 mV) are in *boldface*. *B*, transient current density-voltage curve (*left*) for Nav1.6 with no peptide (*black circles*), CN21 (*red triangles*), and CN21Ala (*gray squares*) in the pipette. Current density values were calculated by normalizing the current amplitude at each voltage by the cell capacitance. Peak current density values are plotted on the *right*. With CN21 treatment, Nav1.6 transient currents are significantly attenuated compared with no peptide and CN21Ala controls ($F(2, 841) = 367.7$, $p < 0.0001$. No peptide and CN21Ala are not significantly different ($p = 0.4800$). ****, $p < 0.0001$. $n = 11–12$. Two-way ANOVA ± S.E. (*error bars*), Tukey's post hoc test.

observed consistent CN21-mediated reductions of Nav1.6 transient and persistent sodium currents in two different cell lines, ND7/23 and HEK293s.

In addition to current density and persistent currents, we also examined whether CaMKII modulates the voltage dependence of activation and steady-state inactivation (channel

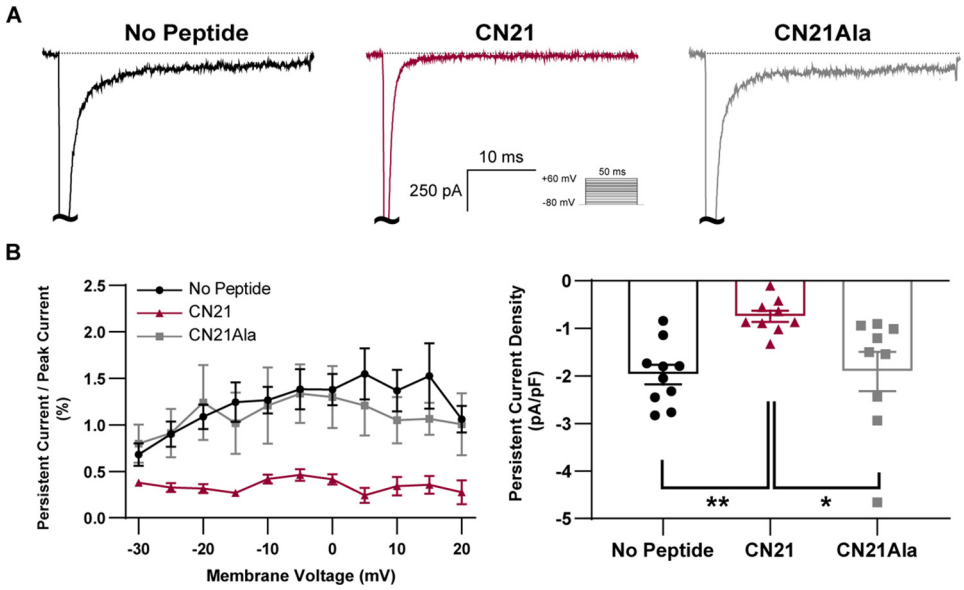

Figure 3. CaMKII inhibition reduces Nav1.6 persistent current density. *A*, representative family of persistent current traces generated by TTX-R hNav1.6 transiently expressed in ND7/23 cells with no peptide (*black*), CN21 (*red*), or CN21Ala (*gray*) in the patch pipette. Currents were elicited with 50-ms step depolarizations ranging from −80 to +60 mV (*inset*) and were measured at 45 ms into the current trace. *B*, percentage persistent current-voltage curve (*left*) for Nav1.6 with no peptide (*black circles*), CN21 (*red triangles*), and CN21Ala (*gray squares*) in the pipette ($F(2, 483) = 45.91$, $p < 0.0001$ with two-way ANOVA). Peak persistent current density values are plotted on the *right* and were calculated by normalizing the current amplitude at each voltage by the cell capacitance. There is a significant reduction of Nav1.6 persistent sodium currents with CaMKII inhibition by CN21 compared with no peptide and CN21Ala controls ($F(2, 267) = 42.07$, $p < 0.0001$). No peptide and CN21Ala persistent currents are not significantly different ($p = 0.9855$). *, $p < 0.05$; **, $p < 0.01$. $n = 9–10$. Two-way ANOVA ± S.E. (*error bars*), Tukey's post hoc test.

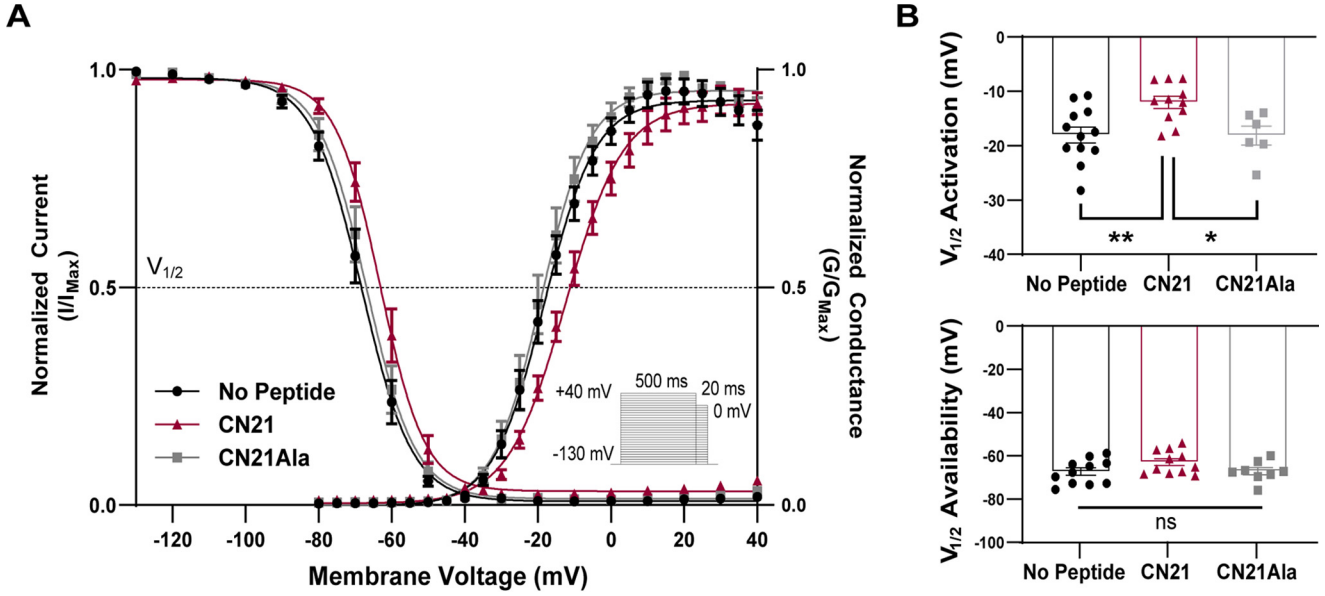

Figure 4. CaMKII inhibition produces a depolarizing shift in Nav1.6 voltage-dependence of activation. *A*, voltage dependence of steady-state activation and inactivation (channel availability) curves fit with a Boltzmann function. Steady-state inactivation was measured by holding cells for 500 ms at a range of prepulse voltages from −130 to +40 mV, followed by a 20-ms test pulse to 0 mV to measure channel availability (*inset*). *B*, activation (*top*) and availability (*bottom*) midpoints. CN21 treatment produced a significant depolarizing shift in the activation midpoint ($F(2, 26) = 6.220$, $p = 0.0062$); however, it had no significant effect on the midpoint of inactivation ($F(2, 29) = 2.229$, $p = 0.126$). *, $p < 0.05$; **, $p < 0.01$; $n = 6–12$. One-way ANOVA ± S.E. (*error bars*), Tukey's post hoc test.

availability) of Nav1.6. Activation and inactivation curves fit with a single Boltzmann function are shown in Fig. 4*A* for Nav1.6 transiently expressed in ND7/23 cells. CaMKII inhibition with CN21 resulted in a significant depolarizing shift in the midpoint for the voltage dependence of activation (Fig. 4*B*, *top*). No significant shifts in channel availability (inactivation midpoint) were observed (Fig. 4*B*, *bottom*). Additionally, we examined the effects of CaMKII inhibition on the ability of Nav1.6 to recover from fast inactivation. No significant shifts in time constants (τ) were observed across treatments (Fig. S2). In total, these data are consistent with CaMKII inhibition producing loss-of-function effects on Nav1.6 channel activity, including decreased transient current density with a proportional decrease in persistent currents relative to the peak transient

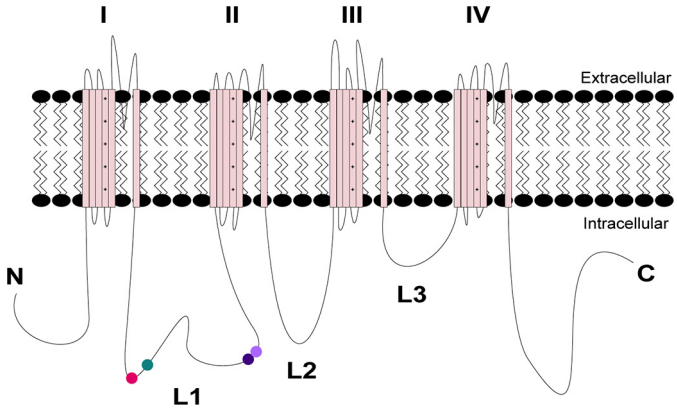

Figure 5. Topology of voltage-gated sodium channel SCN8A. Potential CaMKII phosphorylation sites are shown in L1 and *labeled* as follows: Ser-541 (*pink*), Ser-561 (*green*), Ser-641 (*dark purple*), and Thr-642 (*light purple*).

current, and a depolarizing shift in the voltage dependence of activation.

Identifying novel CaMKII phosphorylation sites on Nav1.6

The α subunit of Nav1.6 is comprised of four transmembrane domains (I–IV), each containing six α-helical segments (S1–S6), with a voltage sensor (S1–S4) and a re-entrant P-loop (S5-S6) that constitutes ion selectivity and the pore of the channel (58). The α subunit contains cytoplasmic N and C termini as well as multiple intracellular loops (L1–L3) that link the four domains (I, II, III, and IV) of the α subunit (Fig. 5). We investigated potential CaMKII phosphorylation of Nav1.6 by immunopurifying it from HEK293 cells stably expressing the channel (59) under conditions promoting and inhibiting CaMKII activity and interrogated Nav1.6 channel phosphorylation via nanoflow LC-ESI/MS (detailed descriptions of all treatments and procedures are outlined under "Experimental procedures"). In these experiments, we compared the phosphorylation status of Nav1.6 in naive cells *versus* cells treated with CaMKII active inhibitors (KN93 overnight at 30 °C and tatCN21 immediately before harvesting) or inactive compounds (KN92 and tatCN21Ala). Whereas we observed 21.5 ± 1.6% autonomously active CaMKII in our Nav1.6-expressing HEK293 cells, which is similar to previously reported values (60), we also exposed these cells to the calcium ionophore ionomycin to promote CaMKII signaling (61) as well as exposing the immunopurified Nav1.6 to recombinant preautophosphorylated (activated) αCaMKII, two treatments that might be expected to maximize CaMKII phosphorylation of Nav1.6. Therefore, a phosphorylation site was considered to be CaMKII-dependent if phosphorylation of that site was observed by nanoflow LC-ESI/MS in both the ionomycin and activated αCaMKII conditions. Phosphosites that were not present in both the ionomycin and activated αCaMKII conditions or were present in the inhibitor condition were likely not phosphorylated by CaMKII and therefore not considered as CaMKII target sites.

Nanoflow LC-ESI/MS analyses of tryptic phosphopeptides revealed an overall coverage (representative coverage map shown in Fig. S3) of the major cytoplasmic regions at 52.5% (513 of 978 amino acids), with 23.5% for the N terminus (31 of 132 amino acids), 64.3% for L1 (222 of 345 amino acids), 42.2% for L2 (94 of 223 amino acids), 52.4% for L3 (33 of 63 amino acids), and 61.9% for the C terminus (133 of 215 amino acids). The identified proteins, Nav1.6 peptide sequences, spectral counts, and amino acid coverage for each experimental condition are shown in Tables S1–S3. Nanoflow LC-ESI/MS analysis under the different conditions led to the identification of eight phosphorylation sites (Table 1). Among the eight phosphosites we repeatedly observed, seven are located in the L1 region of the channel (Ser-504, Ser-541, Ser-561, Ser-579, Ser-589, and Ser-641 and/or Thr-642), and one is located in the C terminus (Ser-1949). Four phosphosites (Ser-504, Ser-579, Ser-589, and Ser-1949) showed measurable phosphorylation across all experimental conditions and were not reactive to CaMKII inhibition by tatCN21/KN93, suggesting that these sites are not sensitive to phosphorylation by CaMKII but are basally phosphorylated in the channel by a different kinase. Bioinformatic screening indicates that Ser-504, Ser-579, and Ser-589 could be targets for casein kinase II phosphorylation, whereas Ser-1949 could be a target for the AGC family of kinases. Potentially four phosphosites (Ser-541, Ser-561, Ser-641, and/or Thr-642) have observable phosphorylation in both ionomycin and preautophosphorylated αCaMKII conditions, suggesting CaMKII-dependent phosphorylation. Fig. 6*A* shows a representative MS/MS spectrum for a singly phosphorylated Nav1.6 peptide at *m*/*z* 695.32 that was fragmented to produce the tandem mass spectrum with b- and y-ion series that correspond to the sequence HNSKSSIFSFR (amino acids 559–569). The b2 and b3 ions unambiguously confirm phosphorylation of residue Ser-561. Fig. 6*B* shows a representative MS/MS spectrum for a phosphorylated Nav1.6 peptide at *m*/*z* 778.50 containing the adjacent sites Ser-641 and Thr-642 that was fragmented to produce the tandem mass spectrum corresponding to the sequence NSTVDCNGVVSLIGGPGSHIGGR (amino acids 640−662). Although the a2 and a3 in addition to the b2 and b3 ions suggest phosphorylation at Thr-642, possible phosphorylation at Ser-641 cannot be discounted. The nonphosphorylated MS/MS spectra corresponding to Fig. 6 are shown in Fig. S4. The MS/MS spectra for the remaining phosphorylated residues listed in Table 1 are shown in Figs. S5–S8.

Navs are large complex transmembrane proteins, which can make them difficult to work with for *in vitro* studies, including technical limitations in obtaining full sequence coverage by MS analysis. Whereas our phosphoproteomic analyses covered over half of the major intracellular regions in Nav1.6, a proportion of these Nav1.6 regions remained uncovered in our spectral analysis. Thus, we sought to experimentally scan each major intracellular region of the channel using immobilized peptide arrays as a complementary method for identifying potential CaMKII phosphorylation sites. Peptides were constructed such that each potential CaMKII phosphorylation site would be represented within multiple peptides (15-mers skipping 4 residues in consecutive peptides), creating multiple opportunities for Ser/Thr phosphorylation by αCaMKII (Fig. 7*A*) to be observed in our peptide arrays. As observed in our nanoflow LC-ESI/MS analysis, Nav1.6 phosphorylation was primarily limited to L1 (Fig. 7*B*) and included Ser-541, Ser-561, and Ser-641/Thr-642 as potential phosphorylation target sites

Table 1

Normalized phosphorylation ratios of identified phosphorylation sites on Nav1.6 by nanoflow LC-ESI/MS analysis. Phosphorylation sites were examined following no treatment, CaMKII inhibition with KN93 and tatCN21, inhibition control with inactive analogues KN92 and tatCN21Ala, ionomycin, and preautophosphorylated αCaMKII treatment (for a detailed description of treatments, see "Experimental procedures"). ND, not determined

Phosphopeptide	Residue	Normalized phosphorylation ratios ± S.E.				
		Naive	KN93 + tatCN21	KN92 + tatCN21Ala	Ionomycin	Preautophosphorylated αCaMKII
		%	%	%	%	%
QKELsEGEEKGDPEK	Ser-504	40.1 ± 14.6	28.5 ± 0.350	46.1 ± 18.6	51.7 ± 31.7	54.5 ± 5.80
FsIMNQSLLSIPGSPFLSR	Ser-541	ND	ND	ND	1.00	10.9 ± 5.00
HNsKSSIFSFR	Ser-561	ND	ND	0.002	4.10 ± 3.30	14.8 ± 10.7
FRDPGsENEFADDEHSTVEESEGRR	Ser-579	39.3 ± 21.1	34.4 ± 13.3	34.9 ± 11.9	27.6 ± 9.10	38.9 ± 14.8
FRDPGsENEFADDEHsTVEESEGRR	Ser-579/Ser-589	19.4 ± 16.1	15.6 ± 9.80	15.2 ± 9.05	6.40 ± 1.80	17.6 ± 12.5
RNstVDC (carbamidomethyl)NGVVSLIGGPGSHIGGR	Ser-641 and/or Thr-642	ND	ND	ND	6.50	31.9 ± 11.7
NstVDC (carbamidomethyl)NGVVSLIGGPGSHIGGR		ND	ND	ND	0.500 ± 0.400	33.6 ± 1.00
KESTPSTASLPSYDsVTKPEKEK	Ser-1949	0.800	0.700	0.600	0.900	10.2

for CaMKII. Moreover, peptides containing Ser-504, Ser-579, Ser-589, and Ser-1949 were not phosphorylated in the array, further supporting our hypothesis that these sites are not CaMKII-dependent. No significant phosphorylation of the N terminus, L2, L3, or C terminus was observed.

To further investigate the contribution of CaMKII phosphorylation at the phosphosites identified in our MS and peptide arrays (Ser-541, Ser-561, Ser-641, and Thr-642), we again used the immobilized peptide arrays to generate mutant peptide phospho-acceptor peptides whereby nonphosphorylatable alanine point mutations of each site were individually tested (Fig. 7*C*). This approach revealed Thr-642 to be the preferential CaMKII target in peptides containing both Ser-641 and Thr-642. Furthermore, similar to our phosphoproteomic analyses, Ser-541 and Ser-561 were again identified as phospho-acceptor sites via site-specific mutagenesis. In total, these data suggest that Ser-541, Ser-561 and Thr-642 are potential candidates for CaMKII phosphorylation regulating CaMKII-dependent functional changes in Nav1.6.

Electrophysiological analysis of CaMKII effects on mutant Nav1.6 activity

To test the role of Ser-541, Ser-561, and Thr-642 in CaMKII regulation of Nav1.6 sodium currents, we again performed whole-cell voltage-clamp on ND7/23 cells transiently expressing mutant forms of hNav1.6. Individual Ala substitutions were introduced at Ser-541, Ser-561, and Thr-642 to mimic a nonphosphorylatable state at these specific residues. For adjacent residues Ser-641 and Thr-642, we chose to introduce Ala at both sites individually and in combination (S641A/T642A) to verify the specificity of our MS and peptide array analyses. To probe CaMKII-specific effects, we included the CaMKII peptide inhibitor CN21 or its inactive analog CN21Ala with Ca^{2+}/CaM in the patch pipette. Our reasoning was that phosphorylation site mutations would be considered CaMKII-specific should the point mutations occlude additional functional effects seen in the presence of the CaMKII inhibitor CN21. To this end, an important CaMKII phosphorylation site would be revealed by a phospho-null mutant decreasing current density in the absence of CN21 while remaining insensitive to CN21 treatment. However, it is conceivable that CN21 effects may not be completely occluded by a single site-specific mutation as we observed previously for the multisite phosphorylation of the cardiac Nav1.5 by CaMKII (57).

A representative family of current traces for S541A, S561A, S641A, T642A, and S641A/T642A treated with no peptide (*left*), CN21 (*middle*), or CN21Ala (*right*) are shown in Fig. S9. Current density curves are shown in Fig. 8*A*, and their peak values within each treatment are plotted in Fig. 8*B*. Substituting an Ala at Ser-541 up-regulates Nav1.6 current density (compared with WT; Fig. 8*B*), suggesting that S541A might prevent a potential phosphorylation site that reduces current density or that this region of L1 is structurally sensitive to mutation. However, treatment with CN21 reduces current density by 36% (compared with no peptide; Fig. 8*B*), indicating that the S541A channel retains sensitivity to current density modulation by CaMKII. Ablation of another potential CaMKII site (S561A) does not alter the current density compared with WT in each treatment (Fig. 8*B*) and retains CN21 sensitivity, displaying a 48% reduction in current density with CaMKII inhibition (Fig. 8*B*). Although less than the current density inhibition observed in the WT channel with CaMKII inhibition, both S541A and S561A still retain CN21 sensitivity.

Further investigation into potential CaMKII modulatory phosphorylation sites in the Nav1.6 L1 domain revealed that introducing an Ala at Ser-641 appears to up-regulate current density in the absence of CaMKII inhibition (compared with WT; Fig. 8*B*), whereas treatment with CN21 reduces its current density by 28% (compared with S641A no peptide; Fig. 8*B*). In contrast, we found that an Ala substitution at the adjacent site Thr-642 reduces current density by 26% in the absence of CaMKII inhibition (compared with WT; Fig. 8*B*) and displays insensitivity to CN21-mediated reductions in current density. Interestingly, introducing Ala at both Ser-641 and Thr-642 in combination (S641A/T642A) displays a 50% reduction in current density. This double mutant, like the single mutant T642A, displays insensitivity to CN21 treatment (Fig. 8*B*) and closely recapitulates the CN21-mediated current density reductions observed in WT. Although significant down-regulation of Nav1.6 persistent currents was observed with CN21 treatment (Fig. 3), we could not explore the effects of point mutants on Nav1.6 persistent currents because peak currents were too small to reliably measure persistent currents in these mutants under our whole-cell voltage-clamp conditions.

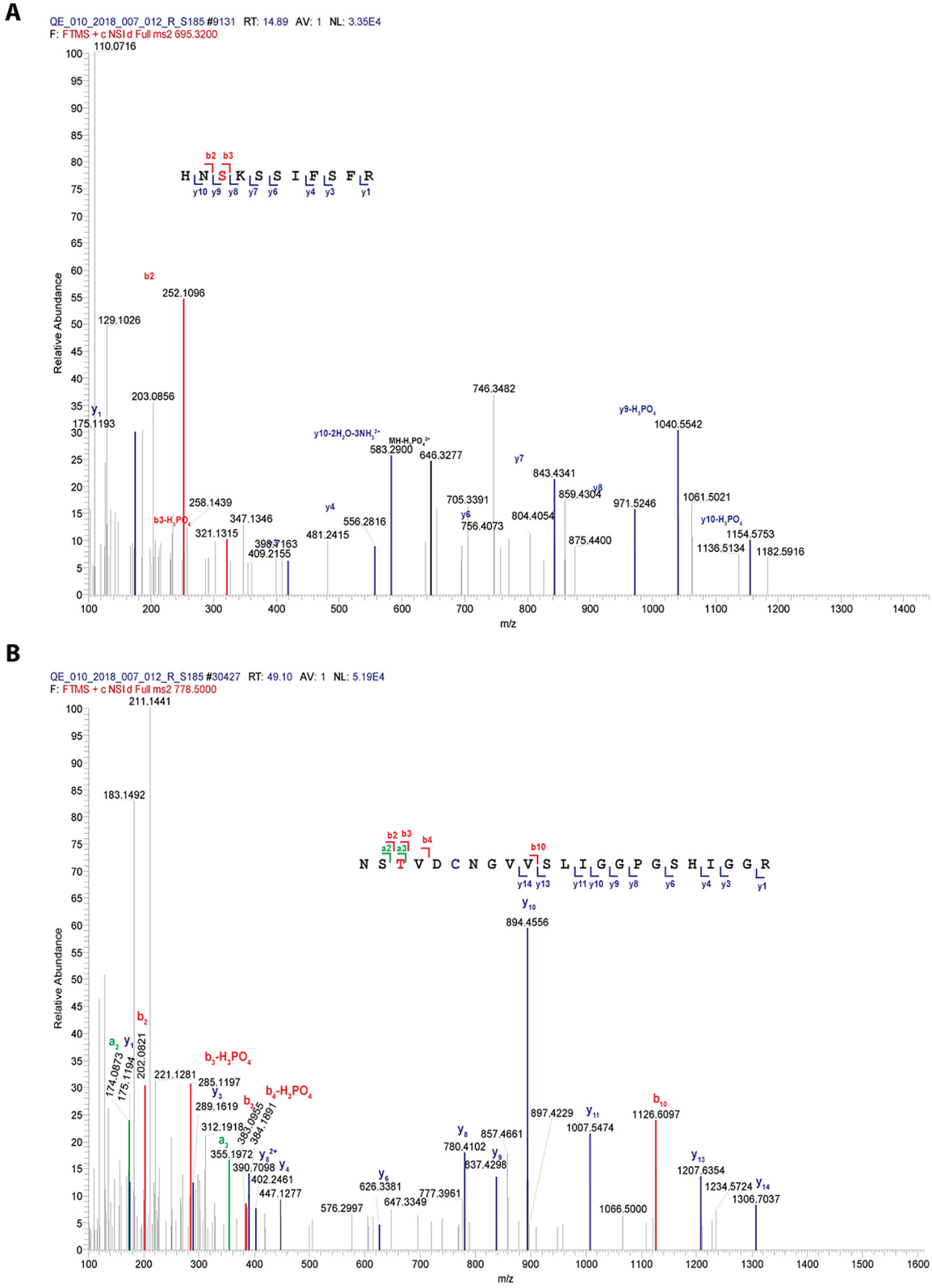

Figure 6. MS/MS spectra for CaMKII phosphorylation sites on Nav1.6 identified by nanoflow LC-ESI/MS. *A*, representative tandem mass spectrum of human Nav1.6 peptide containing pSer-561. The spectrum of a singly phosphorylated Nav1.6 peptide at *m/z* 695.32 was fragmented to produce a tandem mass spectrum with y-ion and b-ion series that correspond to the sequence HNSKSSIFSFR (amino acids 559–569) and confirm the phosphosite at Ser-561. *B*, representative tandem mass spectrum for a phosphorylated Nav1.6 peptide at *m/z* 778.50 containing adjacent sites Ser-641 and Thr-642 that could not be confidently differentiated by MS/MS analysis. The peptide was fragmented to produce the tandem mass spectrum with a-ion and b-ion series that correspond to the sequence NSTVDcNGVVSLIGGPGSHIGGR (amino acids 640–662).

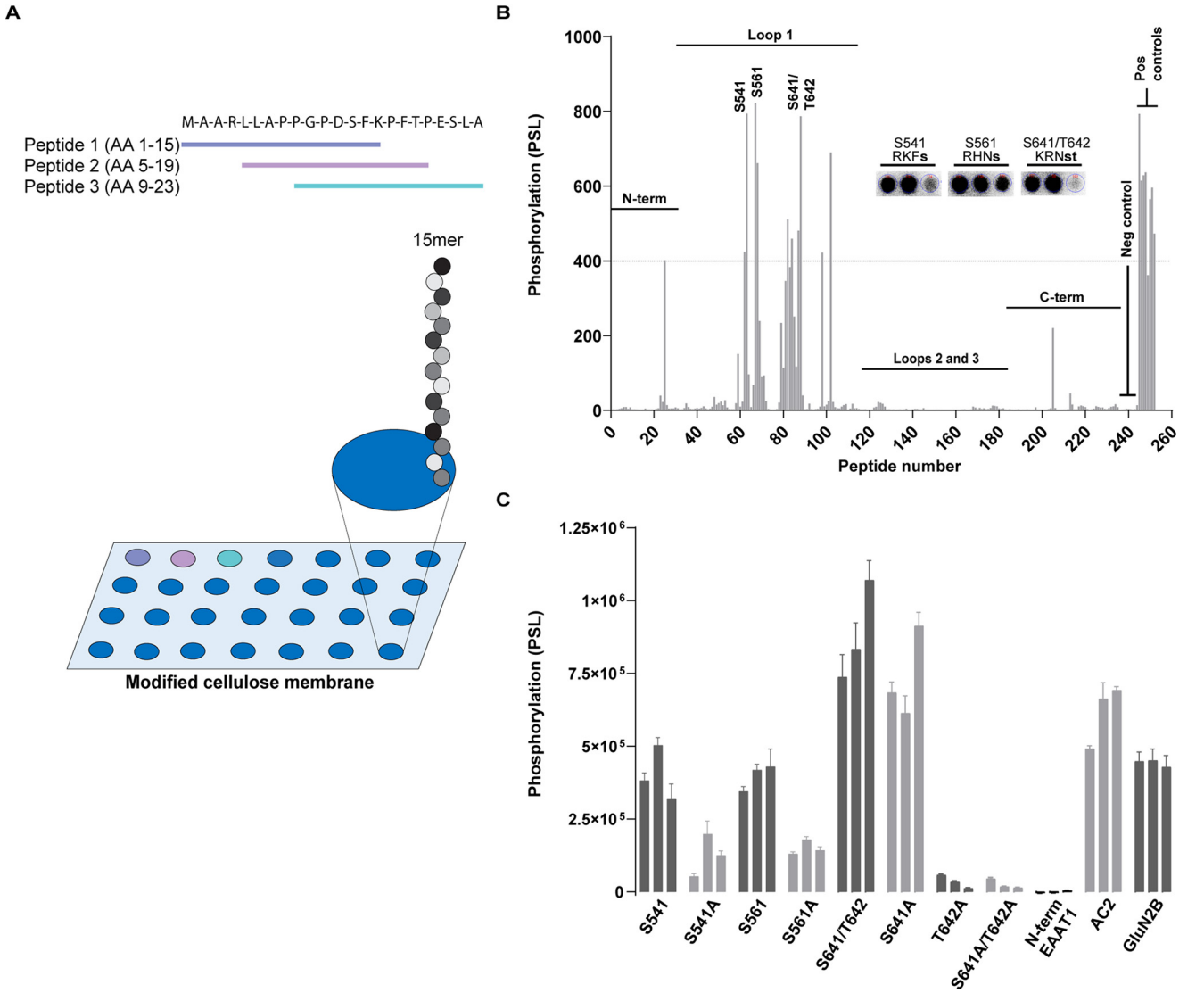

Figure 7. Immobilized peptide arrays of potential CaMKII phosphorylation sites in Nav1.6. *A*, schematic of the SPOTs immobilized peptide tiling assay performed in *B* and *C*. *B*, phosphorylation intensity of peptides tiled from the intracellular regions of human Nav1.6 after αCaMKII phosphorylation with [γ-^{32}P] ATP. Corresponding intracellular regions are *labeled* and *single-letter* amino acid codes/phosphorylation motifs for each putative phosphorylation site are shown. *Inset*, representative phosphor image of immobilized tiled peptide spots (*darkness intensity* indicates ^{32}P incorporation in that peptide). Phosphosites were identified if two or more successive peptides were phosphorylated at the indicated threshold (*dotted line*) of known phosphorylated substrates AC2 and GluN2B (positive controls). *C*, average phosphorylation of immobilized peptides with WT and Ala point mutations introduced at phosphosites identified by peptide array in *B* and nanoflow LC-ESI/MS analysis. Double Ala mutations were introduced at the adjacent sites Ser-641/Thr-642 to identify preferential contribution of CaMKII phosphorylation. The N terminus of EAAT1 served as the negative control; AC2 and GluN2B phosphorylation served as positive controls.

We next explored whether the Ala point mutations at Ser-541, Ser-561, Ser-641, and Thr-642 have any effect on the voltage dependence of activation and channel availability. Voltage dependence of activation and availability curves fit with a single Boltzmann function for WT, S541A, S561A, S641A, T642A, and S641A/T642A Nav1.6 are shown in Fig. 9*A*. An Ala substitution at Ser-561 displays a depolarizing shift in the activation midpoint independent of CaMKII inhibition (Fig. 9*B*), similar to that of WT Nav1.6 treated with CN21. Although there might be a trend for S541A, S641A, and T642A to shift channel activation, none of these mutants, in addition to S641A/T642A, were significantly different from WT. Next, we examined effects of CaMKII nonphosphorylatable point mutants on channel availability. Although we did not observe any significant shifts in WT Nav1.6 treated with CN21, we did observe a trend for S641A/T642A to produce a hyperpolarizing shift in channel availability when compared with WT treated with CN21 (Fig. 9*C*). This effect may be explained by the small depolarizing shift CN21 produces in the WT channel. Last, we examined whether CaMKII nonphosphorylatable point mutants have an effect on the ability for the channel to recover from fast inactivation. Although S641A/T642A produces a significant increase in the recovery time constant (τ) (Fig. S10), this increase does not appear to be CaMKII-dependent, as WT treated with CN21 does not display any changes in recovery from inactivation. These data suggest a complex functional relationship between multiple CaMKII phosphorylation sites within the L1 domain in the modulation of Nav1.6 channel properties.

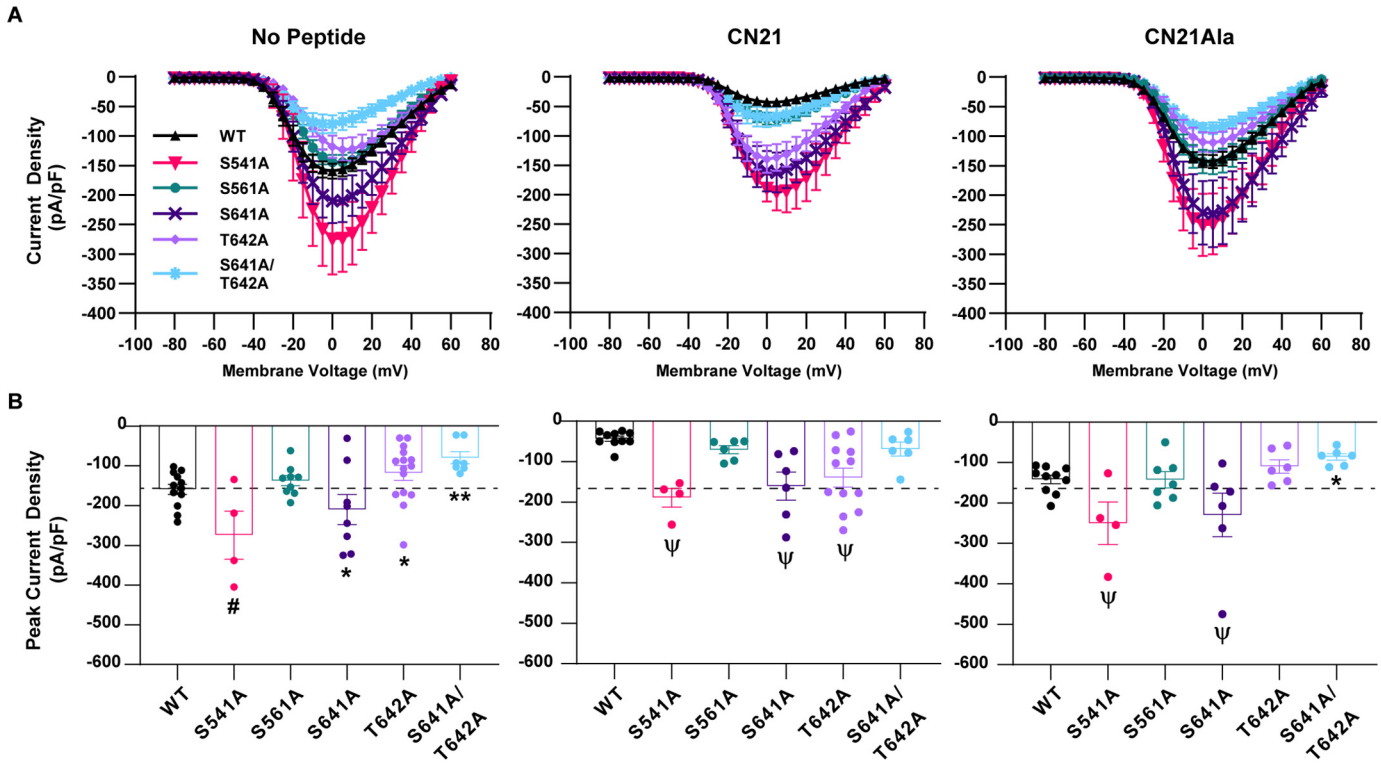

Figure 8. CaMKII modulates Nav1.6 sodium currents at Ser-641/Thr-642. Shown are transient current density-voltage curves (*A*) and corresponding bar graphs (*B*) of peak current densities for Nav1.6 phospho-null mutations with no peptide (*left*), CN21 (*middle*), and CN21Ala (*right*) in the pipette. The *dotted line* serves as a visual control representing Nav1.6 WT current density with no peptide. S541A and S641A increase Nav1.6 current density, whereas T642A and S641A/T642A decrease current density compared with WT Nav1.6 in the absence of CaMKII inhibition, while S561A displayed no change ($F(5, 1419) = 66.84$, $p < 0.0001$ by two-way ANOVA). When treated with CN21, only S561A and S641A/T642A maintain a similar current density to WT Nav1.6 with CN21 treatment ($F(5, 1101) = 91.15$, $p < 0.0001$ by two-way ANOVA). Similar to the no peptide condition, S541A and S641A increased Nav1.6 current density compared with WT treated with CN21Ala whereas S641A/T642A displayed a significant decrease, and S561A displayed no change ($F(5, 956) = 59.17$, $p < 0.0001$). No peptide: S561A *versus* WT, $p = 0.9029$. CN21: S561A *versus* WT, $p = 0.4133$ and S641A/T642A *versus* WT, $p = 0.4861$. CN21Ala: S561A *versus* WT, $p > 0.9999$ and T642A *versus* WT, $p = 0.3856$. *, $p < 0.05$; **, $p < 0.01$; #, $p < 0.001$; Ψ, $p < 0.0001$. $n = 4–15$. Two-way ANOVA ± S.E. (*error bars*), Dunnett's post hoc test *versus* WT within treatment.

Computational simulations of CaMKII modulation of Nav1.6 on action potential firing in Purkinje neurons

We simulated AP firing in a Nav1.6 single-compartment model of a Purkinje neuron (62) to model potential changes in neuronal excitability with CaMKII modulation of Nav1.6. Spontaneous and evoked APs were simulated by adjusting the sodium channel parameters of the Markov state sodium channel model (62) to reflect the functional changes observed in our CN21-treated Nav1.6 channel (CN21 neuron). The default sodium channel parameters of the Khaliq model simulated no peptide treatment (control neuron). Voltage-clamp simulations were performed to validate that the relative CN21-mediated shift in activation and reduction in current density observed in our experimental data were successfully recapitulated in our model (Fig. 10). Simulations of spontaneous action potential frequency in a Purkinje neuron with and without CN21-mediated functional changes to Nav1.6 are shown in Fig. 11*A*. Only the control neuron fired spontaneous action potentials, whereas the CN21 neuron did not spontaneously fire at all. Because our experimental data suggest that the shift in the voltage dependence of activation and reduction in current density produced by CN21 treatment appear to be independently regulated in part by the CaMKII phosphosites Ser-561 and Ser-641/Thr-642, respectively, we next modeled these effects independently to further explore how site-specific CaMKII modulation of Nav1.6 activity impacts excitability. Interestingly, the shift in activation (Ser-561 neuron) or reduction in current density (Ser-641/Thr-642 neuron) alone ablated spontaneous AP firing similar to the CN21 neuron (Fig. 11*A*).

Next, we simulated evoked AP firing in Purkinje neurons. Evoked AP frequency is shown in Fig. 11*B*, and representative traces of those APs are displayed in Fig. 11*C*. Evoked excitability of the CN21 and Ser-641/Thr-642 neurons was profoundly reduced compared with the control and Ser-561 neurons. The Ser-561 neuron was less excitable in response to lower range stimulation; however, its AP firing frequency continued to increase with higher-range stimulation despite never reaching the same AP firing frequency as the control neuron. Intriguingly, the Ser-641/Thr-642 neuron began firing at lower stimulation values than the Ser-561 neuron; however, it maintained low AP firing frequency across the entire range of stimulation, similar to the CN21 neuron. Our simulations demonstrate that the CN21-mediated reduction in current density alone has a stronger impact on neuronal excitability than the change in activation, and, when modeled together, they produce a potentiated inhibition on AP firing. These modeling data reveal that CaMKII modulation of Nav1.6 may have profound effects on neuronal excitability and that distinct CaMKII phosphosites on the channel may differentially tune neuronal excitability in response to neuronal stimuli.

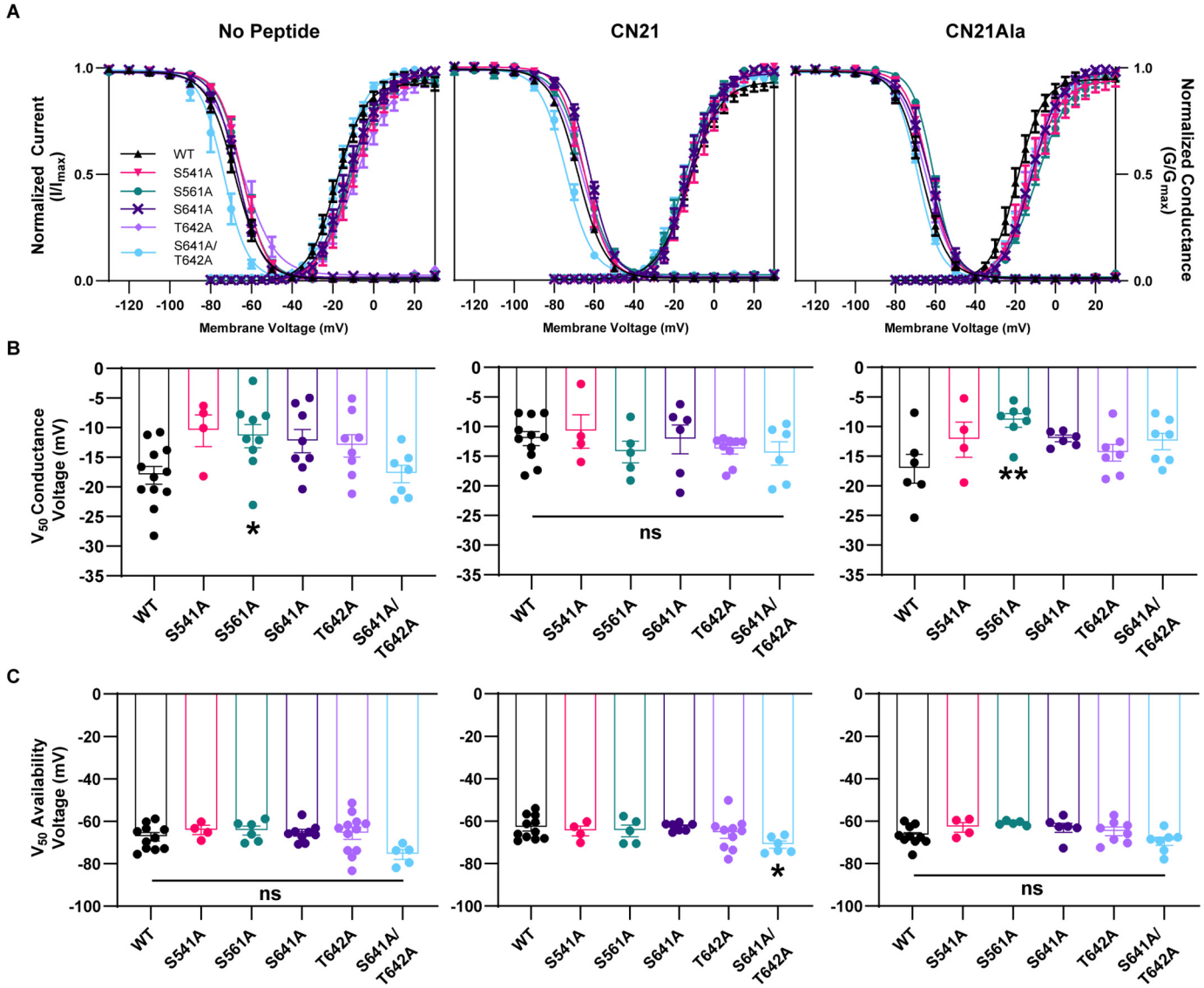

Figure 9. Effects of CaMKII phospho-null mutations in Nav1.6 on voltage-dependence of activation and channel availability. *A*, voltage dependence of steady-state activation and inactivation (channel availability) curves fit with a Boltzmann function comparing WT and phospho-null mutants with no peptide (*left*), CN21 (*middle*), or CN21Ala (*right*) in the patch pipette. Steady-state inactivation was measured by holding cells for 500 ms at a range of prepulse voltages from −130 to +40 mV, followed by a 20-ms test pulse to 0 mV to measure channel availability. *B*, voltage dependence of steady-state activation midpoints. Compared with WT, S561A is the only mutant that displays a significant depolarizing shift in activation midpoint independent of CaMKII inhibition. No peptide: $F(5, 42) = 3.114$, $p = 0.0177$. CN21: $F(5, 35) = 0.6870$, $p = 0.6365$. CN21Ala: $F(5, 31) = 2.865$, $p = 0.0307$. *C*, voltage dependence of steady-state inactivation midpoints. No peptide: $F(5, 41) = 2.392$, $p = 0.0541$. CN21: $F(5, 37) = 2.109$, $p = 0.0861$. CN21Ala: $F(5, 34) = 2.760$, $p = 0.0338$. *, $p < 0.05$; **, $p < 0.01$. n = 4–12. One-way ANOVA ± S.E. (*error bars*), Dunnett's post hoc test (*versus* WT). *Conductance*: no peptide *versus* WT: S541A, $p = 0.0749$; S561A, $p = 0.0304$; S641A, $p = 0.0893$; T642A, $p = 0.1760$; S641A/T642A, $p = 0.9999$. CN21 *versus* WT: S541A, $p = 0.9868$; S561A, $p = 0.8290$; S641A, $p > 0.9999$; T642A, $p = 0.8514$; S641A/T642A, $p = 0.7207$. CN21Ala *versus* WT: S541A, $p = 0.2407$; S561A, $p = 0.0050$; S641A, $p = 0.1456$; T642A, $p = 0.6502$; S641A/T642A, $p = 0.1812$. *Availability*: no peptide *versus* WT: S541A, $p = 0.8900$; S561A, $p = 0.8494$; S641A, $p = 0.9530$; T642A, $p = 0.9620$; S641A/T642A, $p = 0.0889$. CN21 *versus* WT: S541A, $p = 0.9847$; S561A, $p = 0.9824$; S641A, $p = 0.9998$; T642A, $p = 0.7540$; S641A/T642A, $p = 0.0265$. CN21Ala *versus* WT: S541A, $p = 0.5310$; S561A, $p = 0.1049$; S641A, $p = 0.4346$; T642A, $p = 0.8963$; S641A/T642A, $p = 0.6977$.

Discussion

Voltage-gated sodium channels play a critical role by regulating Na^+ permeability across the cellular membrane and are essential for action potential initiation and propagation in excitable cells (3, 63). While there are multiple Nav isoforms with tissue-specific and developmental expression patterns (64, 65), Nav1.6 activity is a well-known and powerful driver of neuronal excitability. Our data demonstrate direct coupling between Nav1.6 function and CaMKII, a critical mediator of synaptic plasticity, learning, and memory (39, 40, 66). We observed that pharmacological CaMKII inhibition in Purkinje neurons significantly reduces transient and persistent sodium currents, indicating that CaMKII modulates sodium currents in neurons. These data are consistent with inhibition of CaMKII impacting excitability in other neuronal paradigms where Nav1.6 is the predominant voltage-gated sodium channel (49), supporting the role of CaMKII as a powerful modulator of neuronal Nav1.6, an isoform predominantly localized to axon initial segments and nodes (3).

Neurons have a complex expression profile for the voltage-gated sodium channel isoforms, and our data are the first to our knowledge to directly demonstrate Nav1.6 modulation by CaMKII. Inhibition of CaMKII in the presence of Ca^{2+} and

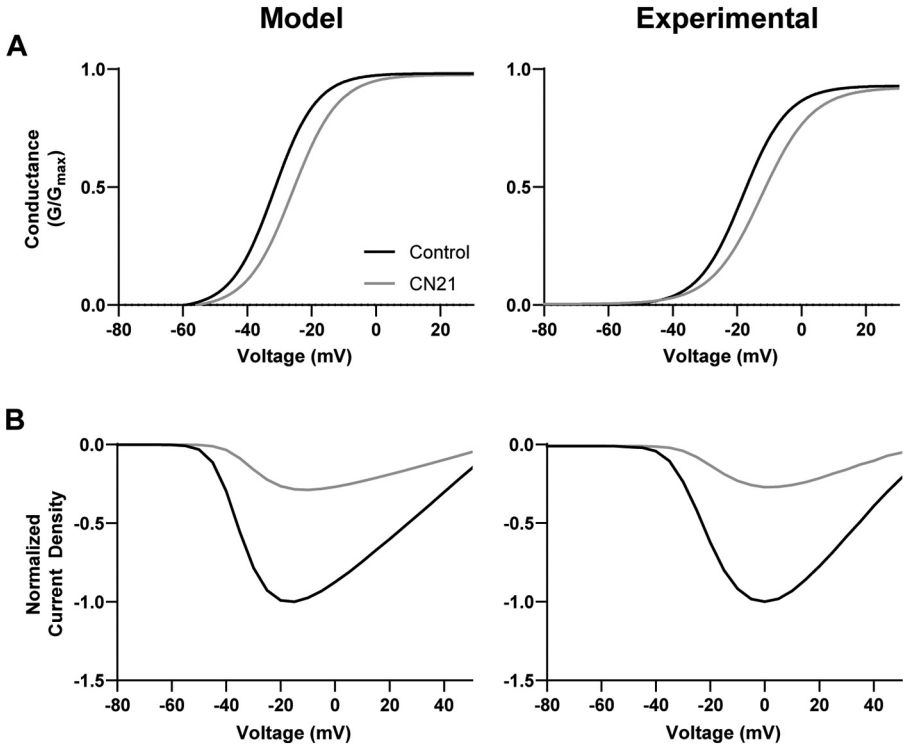

Figure 10. Voltage-clamp simulations of modeled Nav1.6 channels with and without CN21-mediated functional alterations. *A*, voltage dependence of activation; *B*, normalized current density-voltage curves for modeled (*left*) and experimental (*right*) channels. The model exemplifies the relative functional alterations (shift in activation and reduction in current density) that were observed with CN21 treatment in our experimental data.

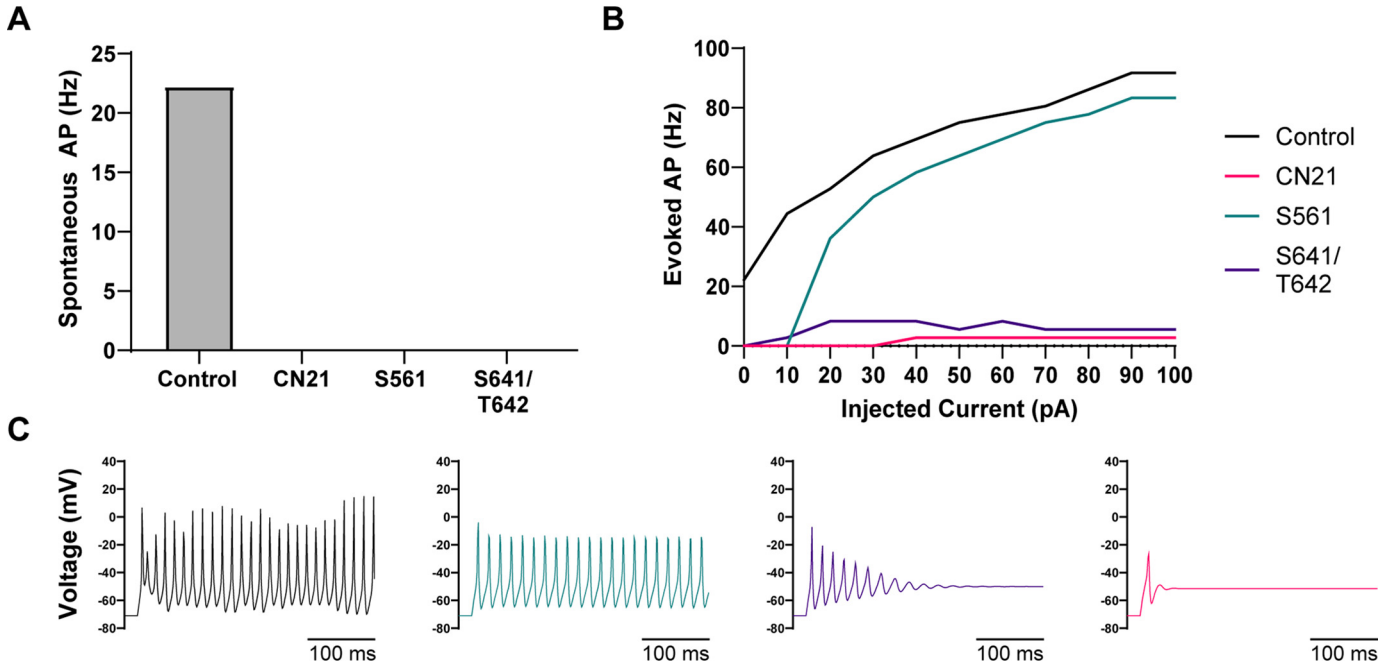

Figure 11. Current-clamp simulations of modeled Nav1.6 channels on action potential firing in simulated Purkinje neurons. Shown is quantification of spontaneous (*A*) and evoked action potential frequency (*B*) from modeled Purkinje neurons with either no peptide control (*black*), CN21 (*pink*), Ser-561 (*teal*), or Ser-641/Thr-642 (*purple*) modeled Nav1.6 currents. Neither the CN21, Ser-561, nor Ser-641/Thr-642 modeled currents fire spontaneous action potentials. Representative traces of evoked action potentials at 40 pA are shown in *C*.

calmodulin in the patch pipette reduced transient and persistent current densities of Nav1.6 in both ND7/23 and HEK293 cells as well as shifted the voltage dependence of activation to more depolarized potentials. Moreover, we show that these functional effects are likely mediated by phosphorylation of Nav1.6 at multiple phosphorylation sites within the L1 loop, Ser-561 and Ser-641/Thr-642, and that each site regulates distinct biophysical characteristics of the channel. We found that

substitution of Ser-561 with an Ala residue is sufficient to recapitulate the CN21-mediated shifts in voltage dependence of activation as observed with CaMKII inhibition. Furthermore, we also determined that whereas the single substitution of Thr-642 with Ala produces an intermediate attenuation of the effects observed with CaMKII inhibition, simultaneous Ala substitutions at both Ser-641 and Thr-642 largely abrogate Nav1.6 current density. Using computational simulations that model the functional phenotypes we observed in our pharmacological and mutant studies, we observed that CaMKII modulation of Nav1.6 is a powerful mediator of neuronal excitability, with phosphorylation sites differentially mediating distinct responses to evoked stimuli. Together, our data suggest that CaMKII modulation of Nav1.6 is a complex and flexible mechanism based on site-specific phosphorylation to regulate neuronal excitability by differentially modulating Nav1.6 function.

Voltage-gated sodium channels undergo multiple post-translational modifications, mechanisms crucial for regulating neuronal input-output properties in physiological and pathological conditions. The phosphorylation of Navs by diverse kinases (*e.g.* PKA, PKC, p38 mitogen-activated protein kinase, and CaMKII) has been shown to modulate several aspects of their function. This kinase diversity represents multiple different signaling pathways that allow Navs to be regulated in combination or uniquely by different second messengers. For example, the regulation of Navs by PKA (cAMP dependence) and PKC (calcium/lipid hydrolysis) has been studied in the greatest detail. Sodium channels from the central nervous system (Nav1.1 and Nav1.2), peripheral nervous system (Nav1.7 and Nav1.8), cardiac tissue (Nav1.5), and skeletal muscle (Nav1.4) are all modulated by PKA and/or PKC and produce differential functional effects (26, 67). Whereas PKC appears to consistently attenuate sodium currents across most isoforms (22, 23, 68–71), the effects of PKA phosphorylation are more diverse, resulting in attenuated Nav1.1 (72), Nav1.2 (25, 73), and Nav1.7 (23) sodium currents while potentiating Nav1.5 (74, 75) and Nav1.8 (23, 76) sodium currents and producing shifts in voltage-dependent gating properties. The PKA phosphosites Ser-573 and Ser-687 (71, 73, 77, 78) and the PKC phosphosite Ser-576 (71) have been shown to underlie functional modulation of Nav1.2 sodium currents. Interestingly, despite carrying homologous PKA and PKC phosphosites, to date Nav1.6 appears to be largely resistant to modulation by these kinases (79). Using multiple approaches, including immobilized peptide arrays and nanoflow LC-ESI/MS, we observed that Ser-561, which is homologous to the PKA phosphosite Ser-573 in Nav1.2, is phosphorylated by αCaMKII. We demonstrate that substituting Ser-561 with an alanine at this position recapitulates the shifts in the voltage dependence of activation with CaMKII inhibition in WT Nav1.6, suggesting that calcium signaling acting through CaMKII may be a powerful mechanism to tune neuronal excitability via regulating Nav1.6 function.

CaMKII is a multifunctional serine/threonine Ca^{2+}-CaM–dependent protein kinase with previous ties to regulating neuronal excitability (29). CaMKII inhibition using the small molecule inhibitor KN93 or KN62 has been observed to decrease sodium currents recorded from cerebellar granule cells (49) and trigeminal ganglion neurons (48), neuronal cells known to express Nav1.6, in addition to decreases in AP firing and amplitude. Moreover, data from our study show that CaMKII inhibition using specific peptide inhibitors decreases both transient and persistent sodium currents in Purkinje neurons, a cell type in which Nav1.6 is predominantly expressed. These data suggest that CaMKII signaling is a powerful modulator of sodium currents produced by neuronal Navs, possibly through modulation of Nav1.6, and may contribute to alterations in AP-firing properties.

A previous report by Belmeguenai *et al.* (80) suggests that AP firing in Purkinje neurons is unaltered in αCaMKII knockout mice. Purkinje neurons express α and βCaMKII as heteromultimeric holoenzymes in an estimated 1:1 ratio (81, 82), with all αCaMKII subunits associating with βCaMKII in Purkinje neurons of WT mice (83). One possibility for unaltered AP firing in Purkinje neurons of αCaMKII knockout mice is functional compensation, because these neurons express multiple isoforms of CaMKII.

Although there are no reports directly investigating CaMKII modulation of Nav1.6 to our knowledge, there are studies exploring the effects of CaMKII modulation of other Nav isoforms in neuronal and cardiac excitability. A recent study has shown that $Scn2a^{Q54}$ mice with a gain-of-function Nav1.2 epilepsy mutation display hyperexcitability that is regulated by CaMKII activity (84). In these mice, CaMKII inhibition results in reduced sodium currents, a shift in availability, and a decrease in the number of APs, implicating CaMKII modulation of Nav1.2 activity with altered excitability. CaMKII modulation of aberrant Nav1.2 activity is underscored by MS data identifying Nav1.2 as a known binding partner of αCaMKII (85); however, the functionally relevant phosphosites contributing to this modulation remain to be determined. In addition to Nav1.2, there is strong evidence for CaMKII modulation of the cardiac isoform Nav1.5 and its potential role in cardiomyocyte excitability (28, 57, 86). Work from our laboratory and others has found that CaMKII phosphorylates Nav1.5 at multiple phosphorylation sites within the L1 domain (57, 87). Our data identifying Nav1.6 L1 as the target for CaMKII phosphorylation are consistent with these reports identifying Nav L1 as a hot spot for CaMKII phosphorylation. CaMKII phosphorylation of Nav1.5 is reported to produce a hyperpolarizing shift in channel availability (57, 88), retard slow inactivation with intermediate kinetics as well as recovery from inactivation, and increase persistent sodium current (89). These effects were abrogated with CaMKII inhibition. Studies have also demonstrated that inhibition of endogenous CaMKII in rat ventricular myocytes results in decreased Nav1.5 sodium current (90). Ashpole *et al.* (57) demonstrated that the CaMKII phosphosites Ser-516 and Thr-594 modulate aspects of Nav1.5 function including channel availability and entry into intermediate inactivation. Notably, the only other Nav isoform with the equivalent Thr-594 site conforming to the CaMKII recognition motif (Arg/Lys-*X*-*X*-Ser/Thr) is Thr-642 of Nav1.6. Using multiple biochemical approaches, we identified Thr-642 as a novel CaMKII phosphosite in HEK293 cells stably expressing Nav1.6. We found that introducing an Ala point mutation at Thr-642 produces an intermediate attenuation of sodium current density, instead of shifting availability as in Nav1.5, independent of

CaMKII inhibition. Although we did not observe significant Ser-641 phosphorylation in our immobilized peptide arrays, we found that introducing an Ala at the adjacent site Ser-641 appears to increase current density in the absence of CaMKII while retaining sensitivity to CaMKII modulation. Moreover, we determined that introducing an Ala at both Ser-641 and Thr-642 reduces sodium current density to a greater degree compared with Thr-642 alone. It is unclear why the double Ala mutation at Ser-641/Thr-642 strongly inhibits sodium current density, whereas the individual Ala substitutions at Ser-641 and Thr-642 independently display a proportion of residual CN21-resistant sodium current. Of course, mutagenesis may sterically alter channel structure and function independent of phospho-null activity. Therefore, if mutagenesis of the Nav1.6 L1 domain at Ser-641/Thr-642 alters the structure of this regulatory hotspot, it might explain the sensitivity of this region to PTMs in addition to why the effects of S641A/T642A are greater than those of either site alone. It is also plausible that disrupting phosphorylation at either Ser-641 or Thr-642 could reveal a third phosphorylation site that opposes the effects of S641A/T642A or promotes channel modulation by another kinase that competes with CaMKII effects on the channel. Further investigation determined that introducing an Ala at another site, Ser-561, did not alter the current density and largely mimicked the WT channel in its response to current density with CN21 treatment, which suggests that this site is not a major determinant in CaMKII modulation of Nav1.6 current density. Alanine mutation at Ser-541 produced a large increase in current density compared with WT; however, this construct retained CN21 sensitivity, thereby remaining partially sensitive to CaMKII activity. Interestingly, recent evaluation of SCN8A in the ClinVar database (RRID:SCR_006169) identified the S541A mutation as a variant (rs753587420) associated with early infantile epileptic encephalopathy. Although S541A is classified as a variant of unknown clinical significance, its association with early infantile epileptic encephalopathy is consistent with the increase in current density we observed, suggesting that the polymorphism S541A alters this regulatory hotspot and may be associated with a gain of function. Further studies may also be required to determine whether Ser-541 phosphorylation could be acting as an opposing brake on current density modulation by CaMKII or a different kinase. If the sites are differentially phosphorylated, it is possible that CaMKII phosphorylation of Ser-541 and Thr-642 may have opposing roles, with Ser-541 contributing to inhibitory tone and Thr-642 to excitatory tone. Whereas none of the phospho-null mutants fully mimicked the current density reduction observed in WT with CN21 treatment, the reduction of current density with phospho-null mutagenesis, coupled with the loss of CN21-mediated reduction as observed in WT, S541A, S561A, and S641A, suggests that Thr-642 phosphorylation and the potential structural sensitivity induced by mutagenesis of the double Ala mutation (S641A/T642A) represents a promising mechanism in the CN21-mediated reductions in WT Nav1.6 sodium current density. Importantly, these data in total show that different isoforms of sodium channels differ in their functional response to phosphorylation at homologous sites by the same kinase, as in the case of CaMKII modulation of Nav1.5 *versus* Nav1.6, or by different kinases, as in Nav1.2 Ser-573 phosphorylation by PKA *versus* the equivalent Ser-561 phosphorylation in Nav1.6 by CaMKII. Whether multiple phosphosites in L1 of Nav1.6 simply represent redundancy or fine tuning of channel function or provide a more complex function like cross-talk between multiple modulatory kinases remains to be determined. Future studies utilizing phosphomimetic substitutions to mimic a negative charge independent of kinase-mediated phosphorylation may be a complementary approach to further dissect the contributions of multisite phosphorylation.

To predict how CaMKII modulation of Nav1.6 may impact excitability at the single-neuron level, we performed computational simulations using a single-compartment Purkinje neuron model (62). We demonstrate that the modeled alterations to channel function due to CaMKII inhibition abrogates spontaneous and evoked AP firing. Because the phospho-null Ala substitutions at Ser-561 and Ser-641/Thr-642 appear to regulate distinct biophysical characteristics of the channel, we extended our model to simulate site-specific modulation of Nav1.6 activity on neuronal excitability. Our simulations demonstrate that targeting the Ser-641/Thr-642–mediated change in current density alone has a greater effect on AP firing frequency than the Ser-561–mediated shift in activation. Importantly, these data reveal that the impact of CaMKII modulation on neuronal excitability can be calibrated by targeting specific residues on Nav1.6 and further demonstrate the remarkable intricacies of Nav modulation.

How can CaMKII modulation of Nav1.6 coordinate responses to synaptic inputs and regulate neuronal excitability? During excitatory events, CaMKII becomes transiently activated in response to Ca^{2+} influx and may retain persistent activity prior to inactivation, providing CaMKII with the unique capability to decode excitatory events and form molecular memory of its activation (39–42). While CaMKII is typically considered important for postsynaptic modulation, such as the postsynaptic density (91, 92), CaMKII is enriched at AISs in neurons and is targeted to the same compartment as Navs via βIV-spectrin/ankyrin-G interactions (28, 30, 31). Previous studies have reported that casein kinase II, which is also localized to the AIS, phosphorylates Nav1.2 and increases the affinity for channel insertion at the AIS in neurons (93). Therefore one might envision a Ca^{2+}-dependent situation where CaMKII phosphorylation of Nav1.6 at Thr-642 may be modulating insertion of channels at the plasma membrane, whereas phosphorylation at Ser-561 may be shifting the activation midpoint of already existing channels, both of which could contribute to increased neuronal excitability. To this end, transient intracellular Ca^{2+} levels at the AIS during physiological activity can increase to ~1.1–3.2 μM (94), which can result in increased local CaMKII activity. A key feature of CaMKII is its ability to decode Ca^{2+} transient frequency into graded levels of activation (95, 96). Importantly, Ca^{2+} transients may greatly vary in frequency, depending on cell type and subcellular compartment. One can speculate that CaMKII activity may produce a graded response on Nav1.6 phosphorylation dependent upon the activation state of CaMKII, which is determined by different patterns of neuronal activity. Conversely, it might be speculated that the loss-of-function effects of Nav1.6 produced by CaMKII inhibition may be adaptive. CaMKII is known to inactivate in

response to prolonged excitotoxic insult (50, 97–100), and therefore this reduction in CaMKII activity may serve a neuroprotective role by keeping Nav1.6 in its unphosphorylated state.

Future studies will be required to determine how the reduction in Nav1.6 current density is triggered with CaMKII inhibition. It is plausible that phosphorylation at Thr-642 stabilizes Nav1.6 channels at the membrane, and upon CaMKII inhibition, a subset of these channels may be internalized from the cell surface through a clathrin-dependent mechanism (101). Ubiquitination of Nav1.6 may also be a possible mechanism mediating decreased current density and triggered by CaMKII inhibition. Nav1.6 contains multiple PY motifs (proline-rich sequence) that allow ubiquitin ligases to bind (102–105), which may in turn be regulated by CaMKII phosphorylation of the channel. Another important level of sodium channel regulation is through phosphatase activity. Multiple studies have demonstrated phosphatase-dependent regulation of CaMKII target proteins (106), including Navs (67). Recent evidence suggests that phosphatases may form macromolecular complexes with Navs and CaMKII in cardiomyocytes, which may contribute to inhibitory balance of CaMKII-dependent modulation of the cardiac isoform Nav1.5 (107). A similar mechanism may be occurring in the context of CaMKII phosphorylation of Nav1.6 such that when CaMKII is inhibited, phosphatase activity may be balancing the inhibitory tone by functioning as a brake on CaMKII activity to differentially control multisite phosphorylation of the channel. Alternatively, alterations to single channel conductance or open probability may also contribute to Nav1.6 modulation by CaMKII. Thus, future studies will need to define how both direct and indirect modes of CaMKII modulation of Nav1.6 may mediate alterations in channel function and expression.

The mechanisms underlying the complex functional effects of CaMKII on Nav1.6 activity are important to elucidate because of their roles in both neuronal physiology and pathology. A recent study identified polymorphisms in the gene encoding αCaMKII, CAMK2A, in autism and epilepsy disorders (32). Likewise, mutations in the gene encoding for Nav1.6, SCN8A, are known to cause excitability disorders as well, particularly severe cases of epilepsy. Whether CaMKII phosphosites in Nav1.6 are phosphorylated simultaneously, sequentially, or individually remains to be determined. Understanding the molecular and structural landscape of Nav1.6 regulation by CaMKII-dependent phosphorylation requires further study; however, our identification of Ser-561 and Thr-642 as functionally important CaMKII phosphosites on Nav1.6 adds valuable insight into the remarkable complexities of channel modulation and possible phospho-dependent changes in neuronal activity.

Experimental procedures

Voltage-gated sodium channel Nav1.6 expression construct and site-directed mutagenesis

Optimized human Nav1.6 encoding the amino acid sequence corresponding to the accession number NP_055006.1 in the NCBI database was designed in our laboratory, synthesized by Genscript, and subcloned into pcDNA3.1 using KpnI and BamHI restriction enzyme sites. Point mutations were introduced into WT tetrodotoxin-resistant Nav1.6 cDNA using the QuikChange II XL site-directed mutagenesis kit from Agilent Technologies following the manufacturer's instructions. Double mutants were carried out sequentially. All mutant channels were fully sequenced with traditional Sanger sequencing (ACGT, Inc.) to confirm the presence of the correct mutation (s) and no additional off-target mutations.

Purkinje neuron acute dissociations

Procedures performed on mice were done in accordance with the Institutional Animal Care and Use Committee–approved protocol. C57/BL6 mice were purchased from Envigo (Indianapolis, IN). These mice were housed under standard conditions with free access to food and water. Acutely dissociated Purkinje neurons were isolated from individual cerebelli of P14–P21 mice of both sexes. Briefly, the vermal layer of the cerebellum was removed and minced. The tissue was then transferred to 5 ml of preoxygenated dissociation solution (82 mM Na_2SO_4, 30 mM K_2SO_4, 5 mM $MgCl_2$, 10 mM HEPES, 10 mM glucose, buffered to pH 7.4 with NaOH) containing 3 mg/ml protease XXIII (Sigma–Aldrich) and incubated for 7 min at 30 °C with constant oxygenation. Following incubation, tissue was washed three times in warmed dissociation solution containing 1 mg/ml BSA (Sigma–Aldrich) to inhibit enzymatic activity. Tissue was then triturated with large-, medium-, and small-diameter fire-polished glass pipettes to liberate individual neurons and plated onto poly-D-lysine (Sigma–Aldrich)–coated 35-mm tissue culture dishes. Plated cells were then incubated in a 5% CO_2 atmosphere at 37 °C for 1 h prior to recording and were recorded from for up to 3 h. For treatments involving tatCN21 and tatCN21Ala, cells were incubated as described previously with tatCN21 or tatCN21Ala (10 μM) (50) for 30 min prior to recordings. Purkinje cells were identified by their large-diameter, pear-shaped cell body and single apical dendrite.

Cell culture

ND7/23 cells (Sigma–Aldrich catalog no. 92090903) were cultured in 4.5 g/liter D-glucose, L-glutamine, and 110 mg/liter sodium pyruvate Dulbecco's modified Eagle's medium (Thermo Fisher Scientific) supplemented with 10% fetal bovine serum (Nucleus Biologicals), penicillin (10 units/ml), and streptomycin (10 μg/ml) at 37 °C in 5% CO_2. Cells were passaged at 85–90% confluence with mechanical dissociation. ND7/23 cells were transiently transfected at 80% confluence using Lipofectamine 2000 (0.5 μl/cm^2; Invitrogen) according to the manufacturer's instructions, with 4 μg of WT or mutant TTX-R channel construct and 250 ng of EGFP (for positive selection) for 4 h, after which the cells were washed and the medium was replaced. Cells were passaged evenly into 4–35-mm cell culture dishes 4 h post-transfection and incubated at 30 °C overnight to increase protein surface expression. Cells were identified by robust expression of EGFP using a fluorescence microscope, and whole-cell patch-clamp recordings were obtained 24–36 h post-transfection. For MS experiments, HEK293 cells (ATCC, CRL-1573) stably expressing human Nav1.6 were used. Stable lines

were maintained in culture medium (described above) with G418 (Sigma–Aldrich, 800 μg/ml). Nav1.6 stable cell lines were generated and characterized in our laboratory.

CaMKII and calmodulin purification

Recombinant αCaMKII was expressed in a baculoviral expression system as described previously (50) with modifications (95). Recombinant calmodulin was expressed and purified in *Escherichia coli* as described previously (95).

Autonomous CaMKII activity assays

ND7/23, HEK293, and Nav1.6-expressing stable HEK293 cultures were briefly rinsed in PBS and lysed in 50 mM HEPES, pH 7.4, 4 mM EGTA, 10 mM EDTA, 15 mM $Na_4P_2O_7{\cdot}10H_2O$, 100 mM β-glycerophosphate, 25 mM NaF, 1% Triton X-100 with phosphatase inhibitors (Calbiochem catalog no. 524624) and protease inhibitors (1 mM 4-benzenesulfonyl fluoride hydrochloride, 300 nM aprotinin, 2 μM E-64, 2 μM leupeptin) as described previously (44, 108). Lysates were sonicated briefly and incubated for 30 min on ice. Ca^{2+}/CaM-dependent CaMKII activity was measured by incubating the lysate with 50 mM HEPES, pH 7.4, 100 mM NaCl, 10 mM $MgCl_2$, 100 μM ATP, 2 mM $CaCl_2$, 5 μM calmodulin, 100 μM AC2 (KKALRRQETVDAL), and [γ-^{32}P]ATP (3 μCi/reaction) for 4 min at 30 °C. Reactions were spotted onto Whatman P81 paper and washed three times for 5 min each in 75 mM phosphoric acid. Radioactivity was quantified via liquid scintillation counting. Ca^{2+}/CaM-independent activity was measured by incubating the lysate under similar conditions, except 5 mM EGTA replaced Ca^{2+}/CaM. Autonomous activity was calculated by the ratio of Ca^{2+}-independent to Ca^{2+}/CaM-dependent activity. To control for nonspecific AC2 phosphorylation in the lysate, reactions were incubated in the absence of AC2. The linear range of the AC2 phosphorylation reactions was greater than 10 min under these conditions.

Peptide SPOTS phosphorylation assays

Standard Fmoc (*N*-(9-fluorenyl)methoxycarbonyl)-protected and activated amino acids (Anaspec, Fremont, CA) were spotted onto derivatized cellulose membranes (PEG linkers; Invatis AG, Cologne, Germany) to create 15-mer peptides synthesized in 20 × 30 peptide arrays using an Invatis MultiPep robot (Cologne, Germany) employing the SPOTS-synthesis method chemistry (109, 110) as described previously (95, 111, 112). Immobilized tiled peptide arrays of Nav1.6 intracellular regions (N terminus, amino acids 1–132; L1, amino acids 409–753; L2, amino acids 977–1199; L3, amino acids 1461–1523; C terminus, amino acids 1766–1980) were tiled, skipping four residues between consecutive peptides (1–15, 5–19, 9–23, etc.). Control peptides were also added to the blot to validate signal intensity between known CaMKII peptide substrates (Autocamtide-2 (AC2), KKALRRQETVDAL; GluN2B, RNKLRRQHSYDTFVD) and peptides that are not phosphorylated by CaMKII (N terminus of EAAT1, MTKSNGEEPKMGGRM). Following synthesis, the membranes were stained with bromphenol blue for annotation and deprotected two times (88% TFA, 2.0% triisopropylsilane, 5.0% phenol, and 5.0% water for 90 min at room temperature), with each deprotection step followed by three 50-ml washes of dichloromethane, three 50-ml washes with dimethylformamide, and three 50-ml washes with ethanol for 5 min each. Before use, the dried membrane was hydrated by exposure to 50 ml of ethanol for 15 min, 50 ml dimethylformamide for 15 min, followed by three washes with 50 ml of PBS. The hydrated blot was then blocked in PBS with 5% filtered BSA (Sigma–Aldrich catalog no. 7030) for 1 h before washing three times with 20 mM Tris, pH 7.4, 200 mM NaCl, 1 mM EDTA, and 0.1% Tween 20 to remove excess blocking agent. The phosphorylation reaction was performed using human αCaMKII (10 nM) in 50 ml of reaction buffer containing 50 mM HEPES, pH 7.4, 100 mM NaCl, 10 mM $MgCl_2$, 0.10 mM ATP, 2 mM $CaCl_2$, 0.000005 mM CaM and 3–6 μCi/ml [γ-^{32}P] ATP for 5 min at room temperature with gentle agitation. The reaction was terminated with three washes of kill buffer (100 mM sodium phosphate, pH 7.0, 1000 mM NaCl, and 10 mM EDTA) (95) and subsequently washed in 75 mM phosphoric acid three times. The phosphorylated peptides were detected using a Fujifilm or an Azure Biosystems phosphorimager. Phosphorylation at each peptide spot was quantified using MultiGauge version 3.1 or the Azure Biosystems Array system. Phosphosites were considered positive if two or more successive peptides were phosphorylated at the indicated threshold of known phosphorylated substrates AC2 and GluN2B (positive controls).

Immunoprecipitation

HEK293 cells stably expressing human Nav1.6 were treated as described below and lysed in 600 μl of 50 mM HEPES, 4 mM EGTA, 10 mM EDTA, 15 mM $Na_4P_2O_7$, 100 mM β-glycerophosphate, 25 mM NaF, 0.1 mM leupeptin, 75 mM μM pepstatin A, 0.1 mg/ml aprotinin, 1% Triton X-100, and 2× protease and phosphatase inhibitor mixtures (Calbiochem), sonicated, and centrifuged at 10,000 rpm for 15 min at 4 °C. Nav1.6 was immunoprecipitated by incubating 10 μg of the monoclonal K58/35 pan-Nav antibody (Sigma–Aldrich, S8809-.1MG) with 1 ml of total lysate at 4 °C overnight. The following day, Protein G–agarose beads (Pierce) were added to the lysate-antibody complex and incubated for 2 h at room temperature. The lysate-antibody-bead complex was subsequently washed five times in lysis buffer and stored in PBS.

Mass spectrometry

CaMKII phosphorylation sites on Nav1.6 were examined with MS by treating Nav1.6-expressing cells with KN93 and tatCN21, KN92 and tatNC21Ala, ionomycin, or autophosphorylated purified αCaMKII. Autophosphorylation of CaMKII was performed in the presence of 50 mM HEPES, pH 7.4, 10 mM $MgCl_2$, 0.5 mM $CaCl_2$, 5 μM CaM, 500 μM ATP with 500 nM recombinant purified αCaMKII for 10 min on ice to autophosphorylate αCaMKII at Thr-286. HEK293 cells stably expressing human Nav1.6 were plated onto 150-mm cell culture dishes and grown to 70% confluence prior to the following treatments. To inhibit CaMKII, cells were treated with a 1 μM concentration of the small molecule CaMKII inhibitor KN93 (Sigma–Aldrich) overnight (or the control compound KN92) at

30 °C. Incubation at 30 °C facilitates maximal membrane expression of the channel as described previously (6). The following day, cells were washed three times with PBS and incubated at 30 °C with 10 μM tatCN21 (50) (or the control peptide tatCN21Ala) in Hanks' balanced salt solution for 20 min prior to cell lysis and immunoprecipitation (described above). To control for temperature-dependent effects, cells were also incubated with no additional treatments (naive treatment group). To promote Ca^{2+}-dependent activation of endogenous CaMKII, cells were treated with 10 μM ionomycin and 2 mM $CaCl_2$ for 5 min in Hanks' balanced salt solution prior to cell lysis and immunoprecipitation. Whereas ionomycin treatment promotes endogenous CaMKII activity, it may also activate other Ca^{2+}-dependent cellular kinases. Therefore, we also treated cell lysates with recombinant autophosphorylated αCaMKII *in vitro*. For this experiment, cells were similarly processed to minimize variation. The Nav1.6-antibody-bead complex was washed with an immunoprecipitation wash buffer containing 50 mM HEPES, 0.1% Tween 20, 100 mM NaCl, 10 mM $MgCl_2$, and 0.5 mM $CaCl_2$ to remove traces of EGTA/EDTA. Autophosphorylated αCaMKII was then added to the washed bead complex and incubated for 10 min at room temperature followed by three washes in PBS. Beads were kept in PBS prior to submission for MS analysis.

Samples were submitted to the Indiana University School of Medicine Proteomics Core Facility for sample processing (described below) and subsequent PTM analysis by nanoflow LC-ESI/MS to identify CaMKII phosphorylation sites on the channel. Following washes, the Nav1.6-antibody-bead complexes were first denatured in 8 M urea and reduced with 5 mM tris(2-carboxyethyl)phosphine hydrochloride, followed by alkylation with 10 mM chloroacetamide. Bead complexes were then incubated with 0.5 μg of trypsin_LysC (Promega) in 2 M urea overnight at 37 °C. Digested peptides were injected onto an Acclaim PepMap C18 trapping column and eluted on a PepMap C18 analytical column with a linear gradient of 3–35% acetonitrile (in water with 0.1% formic acid) and developed over 120 min at room temperature at a flow rate of 700 nl/min. Effluent was electrosprayed into Thermo Dionex UltiMate 3000 RSLC nano system and Velos Pro Orbitrap or Qexactive mass spectrometer. A blank was run prior to each injected sample to ensure there was no significant signal from solvents or the column. Raw files were analyzed using Xcaliber Qual Browser (version 2.2.48), and database searches (Proteome Discoverer version 2.2, SEQUEST XCorr and Scaffold Q) against the human proteome from Uniprot (version downloaded February 15, 2017) were performed with the following parameters: a peptide mass tolerance of 10.0 ppm, fragment mass tolerance of 0.80 Da, trypsin digestion (cleavage after lysine and arginine) allowing two missed cleavages, carbamidomethylation of Cys set as a fixed modification, and oxidation of methionine and phosphorylation (serine, threonine, tyrosine) considered as variable modifications. False discovery rate was set to 1.0%, and peptide spectral matches were accepted if they could be established at >90% probability. Results and quantitative data from each nanoflow LC-ESI/MS analysis are reported in Tables S1 and S2. Each MS/MS spectrum exhibiting possible phosphorylation was manually validated based on an observed 98-Da mass loss ($-H_3PO_4$) for both precursor and fragmented ions using Xcaliber Qual Browser (version 2.2.48). Phosphorylation ratios were measured by normalizing the area under the MS peak to that of the parent peptide identified in all samples for normalization across all conditions.

Whole-cell voltage-clamp recordings

All whole-cell voltage-clamp recordings were obtained at room temperature using a HEKA EPC-10 amplifier and Pulse v9 (HEKA electronic) for data acquisition. For experiments with ND7/23 and HEK293 cells, electrodes were fabricated from 1.7-mm capillary glass and fire-polished to a resistance of 0.8–1.3 megaohms using a Sutter P1000 micropipette puller (Sutter Instrument Co.). The bath solution contained 140 mM NaCl, 1 mM $MgCl_2$, 3 mM KCl, 1 mM $CaCl_2$, 10 mM HEPES and adjusted to pH 7.35 with NaOH and 500 nM TTX to silence endogenous channels (for recordings in Purkinje neurons or HEK293 cells, no TTX was added). Whereas Navs are typically recorded in conditions using fluoride in the patch pipette, a fluoride-free internal solution was used to avoid complications of intracellular fluoride inhibiting calcium signaling and kinase activity (113). The pipette solution contained 10 mM $NaMeSO_3$, 120 mM $CsMeSO_3$, 5 mM EGTA, 10 mM HEPES, 10 mM glucose, 5 mM MgATP, 5 mM $CaCl_2$ and adjusted to pH 7.35 with CsOH (290 mosM). Internal solutions were then aliquoted into single-use aliquots and stored at −80 °C. To promote Ca^{2+}-dependent acute activation of endogenous CaMKII, 1 μM free Ca^{2+} (calculated using WEBMAXC) and calmodulin were included in the internal solution. Calmodulin was added to the solution directly before use. To assess CaMKII-specific effects on Nav1.6 activity, biophysical properties were measured with and without the CaMKII peptide inhibitor CN21 (10 μM) or its inactive analog, CN21Ala (10 μM), in the pipette. Including CN21 in the pipette eliminates the potential for Ca^{2+} and calmodulin effects on Nav1.6 sodium currents and ensures that the effects measured are specific to CaMKII. All voltage protocols were started 5 min after obtaining the gigaohm seal and entering whole-cell configuration to allow for enough time for diffusion of calmodulin and the CN21 or CN21Ala peptides into the cell and to control for time-dependent effects on channel properties. The estimated liquid junction potential for these solutions was <9 mV; data were not corrected to account for this offset. The offset potential was zeroed before the cells were patched. Voltage errors were minimized using >70% series resistance compensation, and passive leak currents were canceled by subtraction. Only cells with a seal resistance of greater than 1 gigaohm were initially selected for analysis. For all recordings involving Purkinje neurons, the tat-conjugated CaMKII inhibitory peptide tatCN21 (10 μM) or the inactive analog tatCN21Ala (10 μM) was incubated in the bath solution for 30 min prior to recording. The same fluoride-free internal solution was used without additional calmodulin in the pipette.

Electrophysiological analysis

Electrophysiological data were analyzed using Pulsefit (version 9.0, HEKA), Microsoft Excel, and Prism (version 8.2, GraphPad Software). For recordings performed in ND7/23 or

HEK293 cells, transient currents were measured during a series of depolarizing steps ranging from −80 to +60 mV for 50 ms from a holding potential of −80 mV. Persistent currents were measured at 45 ms into the depolarizing step and held to strict selection criteria such that each cell analyzed had a seal resistance greater than 1 gigaohm, had a leak current smaller than 50 pA, and displayed inward currents 45 ms into the current trace for greater than 70% of the trace. Persistent current densities were calculated by normalizing the persistent current at each voltage to the cell capacitance. We chose to analyze the persistent currents as a function of cell capacitance (current density) because the currents produced with CN21 treatment were too small in amplitude to reliably measure as a function of the peak transient current (percentage of peak transient current). Persistent current displayed as percentage of peak transient current was used to visualize voltage dependence. For recordings performed in acutely dissociated Purkinje neurons, sodium currents were measured during a series of depolarizing steps ranging from −100 to +15 mV for 50 ms from a holding potential of −100 mV. Sodium current conductance (G_{Na}) was calculated using the equation,

$$G_{Na} = I_{NaT}/(V - V_{rev}) \quad \text{(Eq. 1)}$$

where V_{rev} is the reversal potential of Na^+ obtained in the Pulsefit software (version 9.0, HEKA Electronic) for each individual cell. Activation curves were generated by plotting the normalized conductance against the depolarizing potential and fitting these values with the Boltzmann function,

$$G_{Na}/G_{max} = 1/1+\exp\left((V_{50,act} \pm V)/k_{act}\right) \quad \text{(Eq. 2)}$$

where G_{max} is the maximal Na^+ conductance, $V_{50,act}$ is the half-maximal potential for activation, V is the depolarizing command potential, and k_{act} is the slope factor. The voltage dependence of steady-state inactivation (availability) of Nav1.6 was measured by holding cells for 500 ms at a range of prepulse potentials from −130 to +40 mV, followed by a 20-ms test pulse at 0 mV to measure channel availability. Steady-state inactivation curves were generated by plotting the normalized sodium current against the corresponding prepulse potentials and subsequently fitting these values with the Boltzmann function,

$$I/I_{max} = 1/\left(1+\exp\left((V_{50,inact} \pm V)/k_{inact}\right)\right) \quad \text{(Eq. 3)}$$

where I_{max} is the peak sodium current, $V_{50,inact}$ is the potential at which half of the sodium channels are available for activation, V is the prepulse command potential, and k_{inact} is the slope factor. Recovery from fast inactivation was measured by applying an initial depolarizing step to 0 mV to measure peak current amplitude, followed by a repolarizing step to −80 mV for increasing durations and a final 20-ms test pulse to 0 mV to measure channel availability. Time constants (τ) for recovery from fast inactivation were obtained by plotting the normalized noninactivated sodium currents against the duration of repolarizing steps fitted with a single first-order exponential function.

Simulations

Computational modeling of Nav1.6 channels and simulation of action potential firing were conducted in a single-compartment model of a Purkinje neuron (62) in the NEURON simulation environment (version 7.7.2) (114). Sodium currents were modeled using a Markov state model as described previously (62) with minor adjustments to the kinetic parameters to replicate the relative functional changes observed in our experimental data. Default parameters were used to model the control channel (Nav1.6 with no peptide), and any modifications made were relative to these parameters. To model the relative shift in the voltage dependence of activation, we changed the rate of activation (α) from 150 to 92 and changed the O_{on} rate from 0.75 to 1.3 to match the small but insignificant shift in inactivation we observed. To model the effects on current density, we reduced the default current density of the model from 0.015 to 0.0045 S/cm^2. Curve fitting and quantitative analysis were performed to validate that the experimental changes were successfully recapitulated in our model. Spontaneous and evoked action potential simulations were conducted with and without these modifications to simulate the effects of CaMKII inhibition on neuronal excitability. Neuronal morphology, channel distribution, and kinetic parameters of all other existing channels remained identical to the original model.

Statistics

GraphPad Prism (version 8.2, GraphPad Software) was used for statistical analyses and curve fitting. All data sets were tested for outlier identification using the ROUT method in GraphPad Prism and were subsequently excluded from analysis. The Shapiro–Wilk normality test was used to confirm normal distribution of each data set. The nonlinear least-squares minimization method was used for all fitted curves. All data points are presented as the mean ± S.E., and n is the number of cells used per experiment. Statistical significance was assessed using one- or two-way ANOVA with Dunnett's or Tukey's post hoc test.

Data availability

Data presented and discussed are included in the article. Detailed proteomics data sets, including raw MS data and corresponding Scaffold files, have been deposited in Figshare (10.6084/m9.figshare.12328031.v1, 10.6084/m9.figshare.12328052.v1, 10.6084/m9.figshare.12328295.v1, 10.6084/m9.figshare.12328478.v1, 10.6084/m9.figshare.12330644.v1, and 10.6084/m9.figshare.12330836.v1) and are publicly accessible.

Acknowledgments—We thank Dr. Yanling Pan (Indiana University School of Medicine) for advice on adapting models in NEURON. We are also grateful for Drs. Yanling Pan and Firoj Sahoo for providing invaluable comments on the manuscript.

Author contributions—A. S. Z., A. J. B., T. R. C., and A. H. conceptualization; A. S. Z. and A. H. data curation; A. S. Z., A. J. B., T. R. C., and A. H. software; A. S. Z., A. J. B., A. M. R., T. R. C., and A. H. formal analysis; A. S. Z., T. R. C., and A. H. validation; A. S. Z., T. R. C., and A. H. investigation; A. S. Z. visualization; A. S. Z., A. J. B., T. R. C., and

A. H. methodology; A.S. Z. writing-original draft; A. S. Z., T. R. C., and A. H. project administration; A. S. Z., A. J. B., A. M. R., T. R. C., and A. H. writing-review and editing; A. J. B., T. R. C., and A. H. resources; T. R. C. and A. H. supervision; T. R. C. and A. H. funding acquisition.

Funding and additional information—This work was supported by NINDS, National Institutes of Health, Grants U54NS108874, R01NS053422, and R33DA041876. The content is solely the responsibility of the authors and does not necessarily represent the official views of the National Institutes of Health.

Conflict of interest—The authors declare that they have no conflicts of interest with the contents of this article.

Abbreviations—The abbreviations used are: Nav, voltage-gated sodium channel; AP, action potential; AIS, axon initial segment; CaMKII, calcium/calmodulin-dependent protein kinase II; CaM, calmodulin; TTX, tetrodotoxin; TTX-R, tetrodotoxin-resistant; ESI, electrospray ionization; PKA, protein kinase A; PKC, protein kinase C; AC2, autocamtide-2; GluN2B, *N*-methyl-d-aspartate receptor subunit 2B; EAAT1, excitatory amino acid transporter isoform 1; PTM, post-translational modification; ANOVA, analysis of variance; EGFP enhanced GFP.

References

1. Catterall, W. A. (2012) Voltage-gated sodium channels at 60: structure, function and pathophysiology. *J. Physiol.* **590,** 2577–2589 CrossRef Medline
2. O'Brien, J. E., and Meisler, M. H. (2013) Sodium channel SCN8A ($Na_v1.6$): properties and de novo mutations in epileptic encephalopathy and intellectual disability. *Front. Genet.* **4,** 213 CrossRef Medline
3. Hu, W., Tian, C., Li, T., Yang, M., Hou, H., and Shu, Y. (2009) Distinct contributions of $Na_v1.6$ and $Na_v1.2$ in action potential initiation and backpropagation. *Nat. Neurosci.* **12,** 996–1002 CrossRef Medline
4. Kole, M. H., and Stuart, G. J. (2012) Signal processing in the axon initial segment. *Neuron* **73,** 235–247 CrossRef Medline
5. Wang, X., Zhang, X. G., Zhou, T. T., Li, N., Jang, C. Y., Xiao, Z. C., Ma, Q. H., and Li, S. (2016) Elevated neuronal excitability due to modulation of the voltage-gated sodium channel $Na_v1.6$ by Aβ1–42. *Front. Neurosci.* **10,** 94 CrossRef Medline
6. Patel, R. R., Barbosa, C., Brustovetsky, T., Brustovetsky, N., and Cummins, T. R. (2016) Aberrant epilepsy-associated mutant $Na_v1.6$ sodium channel activity can be targeted with cannabidiol. *Brain* **139,** 2164–2181 CrossRef Medline
7. Bant, J. S., and Raman, I. M. (2010) Control of transient, resurgent, and persistent current by open-channel block by Na channel β4 in cultured cerebellar granule neurons. *Proc. Natl. Acad. Sci. U. S. A.* **107,** 12357–12362 CrossRef Medline
8. Pan, Y., and Cummins, T. R. (2020) Distinct functional alterations in SCN8A epilepsy mutant channels. *J. Physiol.* **598,** 381–401 CrossRef Medline
9. Kole, M. H., and Stuart, G. J. (2008) Is action potential threshold lowest in the axon? *Nat. Neurosci.* **11,** 1253–1255 CrossRef Medline
10. Osorio, N., Cathala, L., Meisler, M. H., Crest, M., Magistretti, J., and Delmas, P. (2010) Persistent $Na_v1.6$ current at axon initial segments tunes spike timing of cerebellar granule cells. *J. Physiol.* **588,** 651–670 CrossRef Medline
11. Xie, W., Strong, J. A., and Zhang, J. M. (2015) Local knockdown of the $Na_V1.6$ sodium channel reduces pain behaviors, sensory neuron excitability, and sympathetic sprouting in rat models of neuropathic pain. *Neuroscience* **291,** 317–330 CrossRef Medline
12. Chen, L., Huang, J., Zhao, P., Persson, A. K., Dib-Hajj, F. B., Cheng, X., Tan, A., Waxman, S. G., and Dib-Hajj, S. D. (2018) Conditional knockout of $Na_V1.6$ in adult mice ameliorates neuropathic pain. *Sci. Rep.* **8,** 3845 CrossRef Medline
13. Laedermann, C. J., Abriel, H., and Decosterd, I. (2015) Post-translational modifications of voltage-gated sodium channels in chronic pain syndromes. *Front. Pharmacol.* **6,** 263 CrossRef Medline
14. Blumenfeld, H., Lampert, A., Klein, J. P., Mission, J., Chen, M. C., Rivera, M., Dib-Hajj, S., Brennan, A. R., Hains, B. C., and Waxman, S. G. (2009) Role of hippocampal sodium channel $Na_v1.6$ in kindling epileptogenesis. *Epilepsia* **50,** 44–55 CrossRef Medline
15. Hargus, N. J., Nigam, A., Bertram, E. H., 3rd, and Patel, M. K. (2013) Evidence for a role of $Na_v1.6$ in facilitating increases in neuronal hyperexcitability during epileptogenesis. *J. Neurophysiol.* **110,** 1144–1157 CrossRef Medline
16. Ottolini, M., Barker, B. S., Gaykema, R. P., Meisler, M. H., and Patel, M. K. (2017) Aberrant sodium channel currents and hyperexcitability of medial entorhinal cortex neurons in a mouse model of SCN8A encephalopathy. *J. Neurosci.* **37,** 7643–7655 CrossRef Medline
17. Butler, K. M., da Silva, C., Shafir, Y., Weisfeld-Adams, J. D., Alexander, J. J., Hegde, M., and Escayg, A. (2017) *De novo* and inherited SCN8A epilepsy mutations detected by gene panel analysis. *Epilepsy Res.* **129,** 17–25 CrossRef Medline
18. Alshammari, M. A., Khan, M. R., Alasmari, F., Alshehri, A. O., Ali, R., Boudjelal, M., Alhosaini, K. A., Niazy, A. A., and Alshammari, T. K. (2019) Changes in the fluorescence tracking of $Na_V1.6$ protein expression in a BTBR T+Itpr3tf/J autistic mouse model. *Neural Plast.* **2019,** 1–12 CrossRef Medline
19. Zhu, H., Lin, W., Zhao, Y., Wang, Z., Lao, W., Kuang, P., and Zhou, H. (2017) Transient upregulation of $Na_v1.6$ expression in the genu of corpus callosum following middle cerebral artery occlusion in the rats. *Brain Res. Bull.* **132,** 20–27 CrossRef Medline
20. Wittmack, E. K., Rush, A. M., Hudmon, A., Waxman, S. G., and Dib-Hajj, S. D. (2005) Voltage-gated sodium channel $Na_v1.6$ is modulated by p38 mitogen-activated protein kinase. *J. Neurosci.* **25,** 6621–6630 CrossRef Medline
21. Wu, J.-X., Tong, L., Hu, L., Xia, C.-M., Li, M., Chen, Q.-H., Chen, F.-X., and Du, D.-S. (2018) Upregulation of $Na_v1.6$ expression in the rostral ventrolateral medulla of stress-induced hypertensive rats. *Hypertens. Res.* **41,** 1013–1022 CrossRef Medline
22. Numann, R., Catterall, W. A., and Scheuer, T. (1991) Functional modulation of brain sodium channels by protein kinase C phosphorylation. *Science* **254,** 115–118 CrossRef Medline
23. Vijayaragavan, K., Boutjdir, M., and Chahine, M. (2004) Modulation of $Na_v1.7$ and $Na_v1.8$ peripheral nerve sodium channels by protein kinase A and protein kinase C. *J. Neurophysiol.* **91,** 1556–1569 CrossRef Medline
24. Tan, Z. Y., Priest, B. T., Krajewski, J. L., Knopp, K. L., Nisenbaum, E. S., and Cummins, T. R. (2014) Protein kinase C enhances human sodium channel $hNa_v1.7$ resurgent currents via a serine residue in the domain III-IV linker. *FEBS Lett.* **588,** 3964–3969 CrossRef Medline
25. Li, M., West, J. W., Lai, Y., Scheuer, T., and Catterall, W. A. (1992) Functional modulation of brain sodium channels by cAMP-dependent phosphorylation. *Neuron* **8,** 1151–1159 CrossRef Medline
26. Cantrell, A. R., and Catterall, W. A. (2001) Neuromodulation of Na^+ channels: an unexpected form of cellular plasticity. *Nat. Rev. Neurosci.* **2,** 397–407 CrossRef Medline
27. Hudmon, A., Choi, J.-S., Tyrrell, L., Black, J. A., Rush, A. M., Waxman, S. G., and Dib-Hajj, S. D. (2008) Phosphorylation of sodium channel $Na_v1.8$ by p38 mitogen-activated protein kinase increases current density in dorsal root ganglion neurons. *J. Neurosci.* **28,** 3190–3201 CrossRef Medline
28. Hund, T. J., Koval, O. M., Li, J., Wright, P. J., Qian, L., Snyder, J. S., Gudmundsson, H., Kline, C. F., Davidson, N. P., Cardona, N., Rasband, M. N., Anderson, M. E., and Mohler, P. J. (2010) A β(IV)-spectrin/CaMKII signaling complex is essential for membrane excitability in mice. *J. Clin. Invest.* **120,** 3508–3519 CrossRef Medline

29. Liu, X. B., and Murray, K. D. (2012) Neuronal excitability and calcium/calmodulin-dependent protein kinase type II: location, location, location. *Epilepsia* **53,** 45–52 CrossRef Medline
30. Grubb, M. S., Shu, Y., Kuba, H., Rasband, M. N., Wimmer, V. C., and Bender, K. J. (2011) Short- and long-term plasticity at the axon initial segment. *J. Neurosci.* **31,** 16049–16055 CrossRef Medline
31. Gasser, A., Ho, T. S., Cheng, X., Chang, K. J., Waxman, S. G., Rasband, M. N., and Dib-Hajj, S. D. (2012) An ankyrinG-binding motif is necessary and sufficient for targeting $Na_v1.6$ sodium channels to axon initial segments and nodes of Ranvier. *J. Neurosci.* **32,** 7232–7243 CrossRef Medline
32. Küry, S., van Woerden, G. M., Besnard, T., Proietti Onori, M., Latypova, X., Towne, M. C., Cho, M. T., Prescott, T. E., Ploeg, M. A., Sanders, S., Stessman, H. A. F., Pujol, A., Distel, B., Robak, L. A., Bernstein, J. A., *et al.* (2017) *De novo* mutations in protein kinase genes CAMK2A and CAMK2B cause intellectual disability. *Am. J. Hum. Genet.* **101,** 768–788 CrossRef Medline
33. Bayer, K. U., and Schulman, H. (2019) CaM kinase: still inspiring at 40. *Neuron* **103,** 380–394 CrossRef Medline
34. Zalcman, G., Federman, N., and Romano, A. (2018) CaMKII isoforms in learning and memory: localization and function. *Front. Mol. Neurosci.* **11,** 445 CrossRef Medline
35. Wang, X., Zhang, C., Szábo, G., and Sun, Q.-Q. (2013) Distribution of CaMKIIα expression in the brain *in vivo*, studied by CaMKIIα-GFP mice. *Brain Res.* **1518,** 9–25 CrossRef Medline
36. Colbran, R. J., Smith, M. K., Schworer, C. M., Fong, Y. L., and Soderling, T. R. (1989) Regulatory domain of calcium/calmodulin-dependent protein kinase II: mechanism of inhibition and regulation by phosphorylation. *J. Biol. Chem.* **264,** 4800–4804 Medline
37. Miller, S. G., and Kennedy, M. B. (1986) Regulation of brain type II Ca^{2+}/calmodulin-dependent protein kinase by autophosphorylation: a Ca^{2+}-triggered molecular switch. *Cell* **44,** 861–870 CrossRef Medline
38. Fong, Y. L., Taylor, W. L., Means, A. R., and Soderling, T. R. (1989) Studies of the regulatory mechanism of Ca^{2+}/calmodulin-dependent protein kinase II: mutation of threonine 286 to alanine and aspartate. *J. Biol. Chem.* **264,** 16759–16763 Medline
39. Hudmon, A., and Schulman, H. (2002) Neuronal Ca^{2+}/calmodulin-dependent protein kinase II: the role of structure and autoregulation in cellular function. *Annu. Rev. Biochem.* **71,** 473–510 CrossRef Medline
40. Lisman, J., Yasuda, R., and Raghavachari, S. (2012) Mechanisms of CaMKII action in long-term potentiation. *Nat. Rev. Neurosci.* **13,** 169–182 CrossRef Medline
41. Coultrap, S. J., and Bayer, K. U. (2012) CaMKII regulation in information processing and storage. *Trends Neurosci* **35,** 607–618 CrossRef Medline
42. Stratton, M., Lee, I. H., Bhattacharyya, M., Christensen, S. M., Chao, L. H., Schulman, H., Groves, J. T., and Kuriyan, J. (2014) Activation-triggered subunit exchange between CaMKII holoenzymes facilitates the spread of kinase activity. *Elife* **3,** e01610 CrossRef Medline
43. Coultrap, S. J., Vest, R. S., Ashpole, N. M., Hudmon, A., and Bayer, K. U. (2011) CaMKII in cerebral ischemia. *Acta Pharmacol. Sin.* **32,** 861–872 CrossRef Medline
44. Ashpole, N. M., Chawla, A. R., Martin, M. P., Brustovetsky, T., Brustovetsky, N., and Hudmon, A. (2013) Loss of calcium/calmodulin-dependent protein kinase II activity in cortical astrocytes decreases glutamate uptake and induces neurotoxic release of ATP. *J. Biol. Chem.* **288,** 14599–14611 CrossRef Medline
45. Yu, H., Pan, B., Weyer, A., Wu, H. E., Meng, J., Fischer, G., Vilceanu, D., Light, A. R., Stucky, C., Rice, F. L., Hudmon, A., and Hogan, Q. (2015) CaMKII controls whether touch is painful. *J. Neurosci.* **35,** 14086–14102 CrossRef Medline
46. Chen, Y., Yang, C., Luo, F., and Wang, Z. (2009) The role of CAMKIIα in neuropathic pain. *J. Pain* **10,** S39 CrossRef
47. Qian, Y., Xia, T., Cui, Y., Chu, S., Ma, Z., and Gu, X. (2019) The role of CaMKII in neuropathic pain and fear memory in chronic constriction injury in rats. *Int. J. Neurosci.* **129,** 146–154 CrossRef Medline
48. Liang, R., Liu, X., Wei, L., Wang, W., Zheng, P., Yan, X., Zhao, Y., Liu, L., and Cao, X. (2012) The modulation of the excitability of primary sensory neurons by Ca^{2+}-CaM-CaMKII pathway. *Neurol. Sci.* **33,** 1083–1093 CrossRef Medline
49. Carlier, E., Dargent, B., De Waard, M., and Couraud, F. (2000) Na^+ channel regulation by calmodulin kinase II in rat cerebellar granule cells. *Biochem. Biophys. Res. Commun.* **274,** 394–399 CrossRef Medline
50. Ashpole, N. M., and Hudmon, A. (2011) Excitotoxic neuroprotection and vulnerability with CaMKII inhibition. *Mol. Cell Neurosci.* **46,** 720–730 CrossRef Medline
51. Taddese, A., and Bean, B. P. (2002) Subthreshold sodium current from rapidly inactivating sodium channels drives spontaneous firing of tuberomammillary neurons. *Neuron* **33,** 587–600 CrossRef Medline
52. Stuart, G., and Sakmann, B. (1995) Amplification of EPSPs by axosomatic sodium channels in neocortical pyramidal neurons. *Neuron* **15,** 1065–1076 CrossRef Medline
53. Schaller, K. L., and Caldwell, J. H. (2003) Expression and distribution of voltage-gated sodium channels in the cerebellum. *Cerebellum* **2,** 2–9 CrossRef Medline
54. Rosker, C., Lohberger, B., Hofer, D., Steinecker, B., Quasthoff, S., and Schreibmayer, W. (2007) The TTX metabolite 4,9-anhydro-TTX is a highly specific blocker of the $Na_{v1.6}$ voltage-dependent sodium channel. *Am. J. Physiol. Cell Physiol.* **293,** C783–789 CrossRef Medline
55. Griffith, T. N., Docter, T. A., and Lumpkin, E. A. (2019) Tetrodotoxin-sensitive sodium channels mediate action potential firing and excitability in menthol-sensitive Vglut3-lineage sensory neurons. *J. Neurosci.* **39,** 7086–7101 CrossRef Medline
56. Herzog, R. I., Liu, C., Waxman, S. G., and Cummins, T. R. (2003) Calmodulin binds to the C terminus of sodium channels $Na_v1.4$ and $Na_v1.6$ and differentially modulates their functional properties. *J. Neurosci.* **23,** 8261–8270 CrossRef Medline
57. Ashpole, N. M., Herren, A. W., Ginsburg, K. S., Brogan, J. D., Johnson, D. E., Cummins, T. R., Bers, D. M., and Hudmon, A. (2012) Ca^{2+}/calmodulin-dependent protein kinase II (CaMKII) regulates cardiac sodium channel $Na_V1.5$ gating by multiple phosphorylation sites. *J. Biol. Chem.* **287,** 19856–19869 CrossRef Medline
58. Catterall, W. A. (2014) Structure and function of voltage-gated sodium channels at atomic resolution. *Exp. Physiol.* **99,** 35–51 CrossRef Medline
59. Pan, Y., Xiao, Y., Pei, Z., and Cummins, T. R. (2020) *S*-Palmitoylation of the sodium channel Nav1.6 regulates its activity and neuronal excitability. *J. Biol. Chem.* **295,** 6151–6164 CrossRef Medline
60. Chawla, A. R., Johnson, D. E., Zybura, A. S., Leeds, B. P., Nelson, R. M., and Hudmon, A. (2017) Constitutive regulation of the glutamate/aspartate transporter EAAT1 by calcium-calmodulin-dependent protein kinase II. *J. Neurochem.* 140, 421–434 CrossRef Medline
61. Tsui, J., Inagaki, M., and Schulman, H. (2005) Calcium/calmodulin-dependent protein kinase II (CaMKII) localization acts in concert with substrate targeting to create spatial restriction for phosphorylation. *J. Biol. Chem.* **280,** 9210–9216 CrossRef Medline
62. Khaliq, Z. M., Gouwens, N. W., and Raman, I. M. (2003) The contribution of resurgent sodium current to high-frequency firing in Purkinje neurons: an experimental and modeling study. *J. Neurosci.* **23,** 4899–4912 CrossRef Medline
63. Catterall, W. A. (2000) From ionic currents to molecular mechanisms: the structure and function of voltage-gated sodium channels. *Neuron* **26,** 13–25 CrossRef Medline
64. Wang, J., Ou, S.-W., and Wang, Y.-J. (2017) Distribution and function of voltage-gated sodium channels in the nervous system. *Channels* **11,** 534–554 CrossRef Medline
65. Black, J. A., and Waxman, S. G. (1996) Sodium channel expression: a dynamic process in neurons and non-neuronal cells. *Dev. Neurosci.* **18,** 139–152 CrossRef Medline
66. Lisman, J. E., and McIntyre, C. C. (2001) Synaptic plasticity: a molecular memory switch. *Curr. Biol.* **11,** R788–R791 CrossRef Medline
67. Scheuer, T. (2011) Regulation of sodium channel activity by phosphorylation. *Semin. Cell Dev. Biol.* **22,** 160–165 CrossRef Medline
68. Numann, R., Hauschka, S. D., Catterall, W. A., and Scheuer, T. (1994) Modulation of skeletal muscle sodium channels in a satellite cell line by protein kinase C. *J. Neurosci.* **14,** 4226–4236 CrossRef

69. Bendahhou, S., Cummins, T. R., Potts, J. F., Tong, J., and Agnew, W. S. (1995) Serine-1321-independent regulation of the mu 1 adult skeletal muscle Na+ channel by protein kinase C. *Proc. Natl. Acad. Sci. U. S. A.* **92,** 12003–12007 CrossRef Medline
70. Qu, Y., Rogers, J., Tanada, T., Scheuer, T., and Catterall, W. A. (1994) Modulation of cardiac Na^+ channels expressed in a mammalian cell line and in ventricular myocytes by protein kinase C. *Proc. Natl. Acad. Sci. U. S. A.* **91,** 3289–3293 CrossRef Medline
71. Cantrell, A. R., Tibbs, V. C., Yu, F. H., Murphy, B. J., Sharp, E. M., Qu, Y., Catterall, W. A., and Scheuer, T. (2002) Molecular mechanism of convergent regulation of brain Na^+ channels by protein kinase C and protein kinase A anchored to AKAP-15. *Mol. Cell. Neurosci.* **21,** 63–80 CrossRef Medline
72. Smith, R. D., and Goldin, A. L. (1998) Functional analysis of the rat I sodium channel in *Xenopus* oocytes. *J. Neurosci.* **18,** 811–820 CrossRef Medline
73. Smith, R. D., and Goldin, A. L. (1997) Phosphorylation at a single site in the rat brain sodium channel is necessary and sufficient for current reduction by protein kinase A. *J. Neurosci.* **17,** 6086–6093 CrossRef Medline
74. Ono, K., Fozzard, H. A., and Hanck, D. A. (1993) Mechanism of cAMP-dependent modulation of cardiac sodium channel current kinetics. *Circ. Res.* **72,** 807–815 CrossRef Medline
75. Matsuda, J. J., Lee, H., and Shibata, E. F. (1992) Enhancement of rabbit cardiac sodium channels by β-adrenergic stimulation. *Circ. Res.* **70,** 199–207 CrossRef Medline
76. Fitzgerald, E. M., Okuse, K., Wood, J. N., Dolphin, A. C., and Moss, S. J. (1999) cAMP-dependent phosphorylation of the tetrodotoxin-resistant voltage-dependent sodium channel SNS. *J. Physiol.* **516,** 433–446 CrossRef Medline
77. Murphy, B. J., Rossie, S., De Jongh, K. S., and Catterall, W. A. (1993) Identification of the sites of selective phosphorylation and dephosphorylation of the rat brain Na^+ channel α subunit by cAMP-dependent protein kinase and phosphoprotein phosphatases. *J. Biol. Chem.* **268,** 27355–27362 Medline
78. Cantrell, A. R., Smith, R. D., Goldin, A. L., Scheuer, T., and Catterall, W. A. (1997) Dopaminergic modulation of sodium current in hippocampal neurons via cAMP-dependent phosphorylation of specific sites in the sodium channel α subunit. *J. Neurosci.* **17,** 7330–7338 CrossRef Medline
79. Chen, Y., Yu, F. H., Sharp, E. M., Beacham, D., Scheuer, T., and Catterall, W. A. (2008) Functional properties and differential neuromodulation of $Na_v1.6$ channels. *Mol. Cell. Neurosci.* **38,** 607–615 CrossRef Medline
80. Belmeguenai, A., Hosy, E., Bengtsson, F., Pedroarena, C. M., Piochon, C., Teuling, E., He, Q., Ohtsuki, G., De Jeu, M. T. G., Elgersma, Y., De Zeeuw, C. I., Jörntell, H., and Hansel, C. (2010) Intrinsic plasticity complements long-term potentiation in parallel fiber input gain control in cerebellar Purkinje cells. *J. Neurosci.* **30,** 13630–13643 CrossRef Medline
81. Walaas, S. I., Lai, Y., Gorelick, F. S., DeCamilli, P., Moretti, M., and Greengard, P. (1988) Cell-specific localization of the α-subunit of calcium/calmodulin-dependent protein kinase II in Purkinje cells in rodent cerebellum. *Brain Res.* **464,** 233–242 CrossRef Medline
82. Hansel, C., de Jeu, M., Belmeguenai, A., Houtman, S. H., Buitendijk, G. H., Andreev, D., De Zeeuw, C. I., and Elgersma, Y. (2006) αCaMKII Is essential for cerebellar LTD and motor learning. *Neuron* **51,** 835–843 CrossRef Medline
83. van Woerden, G. M., Hoebeek, F. E., Gao, Z., Nagaraja, R. Y., Hoogenraad, C. C., Kushner, S. A., Hansel, C., De Zeeuw, C. I., and Elgersma, Y. (2009) βCaMKII controls the direction of plasticity at parallel fiber-Purkinje cell synapses. *Nat. Neurosci.* **12,** 823–825 CrossRef Medline
84. Thompson, C. H., Hawkins, N. A., Kearney, J. A., and George, A. L., Jr. (2017) CaMKII modulates sodium current in neurons from epileptic Scn2a mutant mice. *Proc. Natl. Acad. Sci. U. S. A.* **114,** 1696–1701 CrossRef Medline
85. Wildburger, N. C., Ali, S. R., Hsu, W. C., Shavkunov, A. S., Nenov, M. N., Lichti, C. F., LeDuc, R. D., Mostovenko, E., Panova-Elektronova, N. I., Emmett, M. R., Nilsson, C. L., and Laezza, F. (2015) Quantitative proteomics reveals protein-protein interactions with fibroblast growth factor 12 as a component of the voltage-gated sodium channel 1.2 (Nav1.2) macromolecular complex in mammalian brain. *Mol. Cell. Proteomics* **14,** 1288–1300 CrossRef Medline
86. Herren, A. W., Bers, D. M., and Grandi, E. (2013) Post-translational modifications of the cardiac Na channel: contribution of CaMKII-dependent phosphorylation to acquired arrhythmias. *Am. J. Physiol. Heart Circ. Physiol.* **305,** H431–H445 CrossRef Medline
87. Herren, A. W., Weber, D. M., Rigor, R. R., Margulies, K. B., Phinney, B. S., and Bers, D. M. (2015) CaMKII phosphorylation of $Na_V1.5$: novel *in vitro* sites identified by mass spectrometry and reduced S516 phosphorylation in human heart failure. *J. Proteome Res.* **14,** 2298–2311 CrossRef Medline
88. Wagner, S., Dybkova, N., Rasenack, E. C., Jacobshagen, C., Fabritz, L., Kirchhof, P., Maier, S. K., Zhang, T., Hasenfuss, G., Brown, J. H., Bers, D. M., and Maier, L. S. (2006) Ca^{2+}/calmodulin-dependent protein kinase II regulates cardiac Na^+ channels. *J. Clin. Invest.* **116,** 3127–3138 CrossRef Medline
89. Maltsev, V. A., Reznikov, V., Undrovinas, N. A., Sabbah, H. N., and Undrovinas, A. (2008) Modulation of late sodium current by Ca^{2+}, calmodulin, and CaMKII in normal and failing dog cardiomyocytes: similarities and differences. *Am. J. Physiol. Heart Circ. Physiol.* **294,** H1597–H1608 CrossRef Medline
90. Yoon, J. Y., Ho, W. K., Kim, S. T., and Cho, H. (2009) Constitutive CaMKII activity regulates Na^+ channel in rat ventricular myocytes. *J. Mol. Cell. Cardiol.* **47,** 475–484 CrossRef Medline
91. Hell, J. W. (2014) CaMKII: claiming center stage in postsynaptic function and organization. *Neuron* **81,** 249–265 CrossRef Medline
92. Petersen, J. D., Chen, X., Vinade, L., Dosemeci, A., Lisman, J. E., and Reese, T. S. (2003) Distribution of postsynaptic density (PSD)-95 and Ca^{2+}/calmodulin-dependent protein kinase II at the PSD. *J. Neurosci.* **23,** 11270–11278 CrossRef Medline
93. Bréchet, A., Fache, M. P., Brachet, A., Ferracci, G., Baude, A., Irondelle, M., Pereira, S., Leterrier, C., and Dargent, B. (2008) Protein kinase CK2 contributes to the organization of sodium channels in axonal membranes by regulating their interactions with ankyrin G. *J. Cell Biol.* **183,** 1101–1114 CrossRef Medline
94. Bender, K. J., and Trussell, L. O. (2009) Axon initial segment Ca^{2+} channels influence action potential generation and timing. *Neuron* **61,** 259–271 CrossRef Medline
95. Johnson, D. E., and Hudmon, A. (2017) Activation state-dependent substrate gating in Ca^{2+}/calmodulin-dependent protein kinase II. *Neural Plast.* **2017,** 9601046 CrossRef Medline
96. De Koninck, P., and Schulman, H. (1998) Sensitivity of CaM kinase II to the frequency of Ca^{2+} oscillations. *Science* **279,** 227–230 CrossRef Medline
97. Aronowski, J., Grotta, J. C., and Waxham, M. N. (1992) Ischemia-induced translocation of Ca^{2+}/calmodulin-dependent protein kinase II: potential role in neuronal damage. *J. Neurochem.* **58,** 1743–1753 CrossRef Medline
98. Hudmon, A., Aronowski, J., Kolb, S. J., and Waxham, M. N. (1996) Inactivation and self-association of Ca^{2+}/calmodulin-dependent protein kinase II during autophosphorylation. *J. Biol. Chem.* **271,** 8800–8808 CrossRef Medline
99. Tao-Cheng, J. H., Vinade, L., Pozzo-Miller, L. D., Reese, T. S., and Dosemeci, A. (2002) Calcium/calmodulin-dependent protein kinase II clusters in adult rat hippocampal slices. *Neuroscience* **115,** 435–440 CrossRef Medline
100. Ashpole, N. M., Song, W., Brustovetsky, T., Engleman, E. A., Brustovetsky, N., Cummins, T. R., and Hudmon, A. (2012) Calcium/calmodulin-dependent protein kinase II (CaMKII) inhibition induces neurotoxicity via dysregulation of glutamate/calcium signaling and hyperexcitability. *J. Biol. Chem.* **287,** 8495–8506 CrossRef Medline
101. Liu, C., Cummins, T. R., Tyrrell, L., Black, J. A., Waxman, S. G., and Dib-Hajj, S. D. (2005) CAP-1A is a novel linker that binds clathrin and the voltage-gated sodium channel $Na_v1.8$. *Mol. Cell. Neurosci.* **28,** 636–649 CrossRef Medline
102. Abriel, H., Kamynina, E., Horisberger, J. D., and Staub, O. (2000) Regulation of the cardiac voltage-gated Na^+ channel (H1) by the ubiquitin-protein ligase Nedd4. *FEBS Lett.* **466,** 377–380 CrossRef Medline
103. Abriel, H., and Staub, O. (2005) Ubiquitylation of ion channels. *Physiology* **20,** 398–407 CrossRef Medline

104. Staub, O., Dho, S., Henry, P., Correa, J., Ishikawa, T., McGlade, J., and Rotin, D. (1996) WW domains of Nedd4 bind to the proline-rich PY motifs in the epithelial Na^+ channel deleted in Liddle's syndrome. *EMBO J.* **15,** 2371–2380 CrossRef Medline
105. Staub, O., Gautschi, I., Ishikawa, T., Breitschopf, K., Ciechanover, A., Schild, L., and Rotin, D. (1997) Regulation of stability and function of the epithelial Na^+ channel (ENaC) by ubiquitination. *EMBO J.* **16,** 6325–6336 CrossRef Medline
106. Baucum, A. J., 2nd, Strack, S., and Colbran, R. J. (2012) Age-dependent targeting of protein phosphatase 1 to Ca^{2+}/calmodulin-dependent protein kinase II by spinophilin in mouse striatum. *PLoS ONE* **7,** e31554 CrossRef Medline
107. Refaey, M. E., Musa, H., Murphy, N. P., Lubbers, E. R., Skaf, M., Han, M., Cavus, O., Koenig, S. N., Wallace, M. J., Gratz, D., Bradley, E., Alsina, K. M., Wehrens, X. H. T., Hund, T. J., and Mohler, P. J. (2019) Protein phosphatase 2A regulates cardiac Na^+ channels. *Circ. Res.* **124,** 737–746 CrossRef Medline
108. Kolb, S. J., Hudmon, A., and Waxham, M. N. (1995) Ca^{2+}/calmodulin kinase II translocates in a hippocampal slice model of ischemia. *J. Neurochem.* **64,** 2147–2156 CrossRef Medline
109. Frank, R., and Overwin, H. (1996) SPOT synthesis: epitope analysis with arrays of synthetic peptides prepared on cellulose membranes. *Methods Mol. Biol.* **66,** 149–169 CrossRef Medline
110. Frank, R. (2002) The SPOT-synthesis technique: synthetic peptide arrays on membrane supports–principles and applications. *J. Immunol. Methods* **267,** 13–26 CrossRef Medline
111. Wang, Q., Chen, M., Schafer, N. P., Bueno, C., Song, S. S., Hudmon, A., Wolynes, P. G., Waxham, M. N., and Cheung, M. S. (2019) Assemblies of calcium/calmodulin-dependent kinase II with actin and their dynamic regulation by calmodulin in dendritic spines. *Proc. Natl. Acad. Sci. U. S. A.* **116,** 18937–18942 CrossRef Medline
112. Shugg, T., Johnson, D. E., Shao, M., Lai, X., Witzmann, F., Cummins, T. R., Rubart-Von-der Lohe, M., Hudmon, A., and Overholser, B. R. (2018) Calcium/calmodulin-dependent protein kinase II regulation of IKs during sustained β-adrenergic receptor stimulation. *Heart Rhythm* **15,** 895–904 CrossRef Medline
113. Vargas, G., Yeh, T. Y., Blumenthal, D. K., and Lucero, M. T. (1999) Common components of patch-clamp internal recording solutions can significantly affect protein kinase A activity. *Brain Res.* **828,** 169–173 CrossRef Medline
114. Hines, M. L., and Carnevale, N. T. (1997) The NEURON simulation environment. *Neural Comput.* **9,** 1179–1209 CrossRef Medline